agriculture

MDPI

Article

Geometry-Optimized Strip Tillage for Improving Soil Physical Quality and Hydraulic Function in Semi-Arid Vineyards

Yurii Syromiatnykov [1,*], Farmon Mamatov [2], Antonina Sholoiko [3,*], Ivan Galych [4], Dilmurod Irgashev [2], Khamrokul Ravshanov [2], Nargiza Ravshanova [2], Gayrat Ergashov [2], Yarash Rajabov [5], Feruza Mukumova [6], Alisher Suyunov [2] and Bektosh Aliev [2]

[1] Institute of Soil and Plant Sciences, Latvia University of Life Sciences and Technologies, 3001 Jelgava, Latvia
[2] Department of Agricultural Engineering, Karshi State Technical University, Karshi 180100, Uzbekistan
[3] Department of Insurance, Banking and Risk Management, Faculty of Economics, Taras Shevchenko National University of Kyiv, 01601 Kyiv, Ukraine
[4] Department of Agricultural Engineering, Faculty of Mechatronics and Engineering, State Biotechnological University, 61000 Kharkiv, Ukraine
[5] Department of Agricultural and Water Management Engineering Technologies, Faculty of Natural Resources Management, Bukhara State Technical University, Buhara 200100, Uzbekistan
[6] Department of Technological Education, Termez State University, Termez 190111, Uzbekistan
* Correspondence: yurii.syromiatnykov@lbtu.lv (Y.S.); sholoiko@knu.ua (A.S.)

Abstract

Soil compaction and reduced infiltration capacity are critical constraints limiting soil physical quality and hydraulic functioning in semi-arid vineyard systems subjected to repeated machinery traffic. This study aimed to develop and evaluate a geometry-optimized strip tillage tool designed to improve structural functionality within the compacted root zone while minimizing inter-row disturbance. A U-shaped working body configuration, consisting of two oppositely inclined shanks and a central chisel, was theoretically substantiated and optimized using multifactor analysis. Field experiments were conducted to assess changes in penetration resistance, bulk density, and infiltration rate within the 20–40 cm soil layer under semi-arid conditions. The optimized geometry significantly reduced penetration resistance and bulk density in the trafficked strip, indicating alleviation of mechanical impedance and improved root-relevant physical conditions. Infiltration capacity increased after treatment, indicating enhanced hydraulic continuity within the root zone. Unlike full-width subsoiling, the localized strip intervention preserved inter-row soil stability and limited unnecessary disturbance, which is consistent with conservation-oriented soil management. The results indicate that geometry-optimized strip tillage is associated with improved soil physical quality and hydraulic function within compacted vineyard strips. The operational applicability of the developed implement may also depend on vineyard layout and terrain conditions. The prototype tool was tested under conditions representative of vineyards with standard row spacing and relatively moderate slopes typical for the experimental site. In vineyards with very narrow row spacing, steep slopes, or highly heterogeneous soil conditions, adjustments in working width, shank spacing, or tractor–implement configuration may be required. Future studies should therefore investigate the performance of the optimized geometry under contrasting vineyard configurations, including steep hillside vineyards and high-density planting systems. By linking implement design to quantitative soil structural and hydraulic indicators, this study contributes to the development of vineyard soil management practices for semi-arid perennial cropping systems.

Academic Editor: Daniel Bucur

Received: 14 February 2026
Revised: 18 March 2026
Accepted: 21 March 2026
Published: 28 March 2026

Copyright: © 2026 by the authors. Licensee MDPI, Basel, Switzerland. This article is an open access article distributed under the terms and conditions of the Creative Commons Attribution (CC BY) license.

Keywords: soil physical quality; hydraulic function; strip tillage; soil compaction; root-zone loosening; infiltration rate; vineyard soil management; semi-arid agriculture; sustainable tillage systems

1. Introduction

Sustainable agriculture in arid and semi-arid regions increasingly depends on practices that improve soil physical quality and hydraulic functioning, because soil structure degradation directly limits infiltration, root access to moisture, and resilience under climate stress. In mechanically managed agroecosystems, the physical state of the root zone is strongly shaped by the design of tillage tools and by operational decisions that determine how stresses are transmitted into the soil profile. Recent advances in implement development demonstrate that geometry-driven design can improve field performance, but the link between tool optimization and measurable soil–water responses still requires more targeted, system-specific evidence, especially for perennial crops.

Engineering solutions for soil loosening and seedbed preparation have typically been developed within annual cropping systems, where combined tools and levelling devices are optimized to improve tilth while controlling traction demand and operational stability. For example, combined tillage solutions and follow-up implementations for melon cultivation illustrate how working body geometry and kinematics can be tuned to reduce passes and enhance soil preparation quality under practical constraints [1,2]. Similarly, rationalization of ridge-related tillage elements emphasizes that parameter selection governs both soil fragmentation and energy consumption in field conditions [3]. More specialized loosening elements, such as ripper–mole knives, highlight how targeted subsurface action can create preferential pathways that influence water movement and structural persistence after the pass [4]. In parallel, non-traditional rotary working bodies further confirm that structural–technological substantiation of geometry can shift the balance between aggregate breakup and resistance, providing additional design concepts that can be transferred across crop systems [5].

Digital design workflows and simulation-based selection have become increasingly important in shortening development cycles and improving reliability of agricultural implements. Computer-aided engineering approaches and simulation-supported material selection have been demonstrated as effective routes to optimize components under load while maintaining manufacturability and durability [6,7]. At the same time, experimental and methodological work on rotary loosening and separating machines underlines that detailed studies of soil–tool interaction and working organ geometry remain essential for understanding fragmentation and flow mechanisms that ultimately affect soil physical status [8]. Precision-oriented deep placement and tree-layer applications also show that targeted, site-specific in-soil operations can be integrated with soil management goals, linking mechanical design with agronomic outcomes [9]. Beyond cropping, even the mechanization of manure handling reflects how technology choice and working actions influence the physical properties of soil amendments and the field environment they are applied to, indirectly shaping soil structure and water dynamics [10].

From a soil physics perspective, compaction and mechanical impedance are central constraints on root-zone function. Straw and residue management can partially mitigate compaction and improve crop performance, but these benefits are conditional on the soil structural context and the degree of traffic-induced densification [11]. Field evidence indicates that repeated machinery passages measurably increase compaction under operational conditions, reinforcing the need for traffic-aware tillage strategies that protect structural porosity and hydraulic conductivity [12]. Mechanistic analyses of edaphic re-

https://doi.org/10.3390/agriculture16070751

sponse to mechanical perturbation further emphasize that soil behavior under tillage is not only a matter of draft force but also of fracture propagation, aggregate rearrangement, and post-tillage structural recovery [13]. Empirical observations of soil density changes under mouldboard-based systems illustrate how conventional approaches can maintain or exacerbate dense horizons that reduce infiltration and root penetration, particularly when management is not explicitly conservation-oriented [14]. These challenges motivate the development of controlled, localized interventions that restore the structural function of the soil while minimizing unnecessary disturbance.

A key direction in sustainable intensification is the integration of tillage with nutrient and amendment placement, because soil structure and water movement mediate nutrient use efficiency. Deep placement of nitrogen fertilizers has been shown to reduce ammonia volatilization and increase nitrogen utilization under no-tillage paddy conditions, highlighting how subsurface placement interacts with soil aeration and moisture regimes [15]. On-farm evidence similarly indicates that fertilizer deep placement can increase rice production, supporting the broader idea that targeted subsurface operations can improve resource efficiency when matched to soil constraints [16]. In other systems, combined applications of herbicides, nitrogen fertilizers, and humic growth regulators affect both weed control and yield in winter wheat, illustrating how soil management and inputs jointly shape productivity outcomes [17]. Engineering developments relevant to manure incorporation and sealing also underscore that parameter selection for subsurface action can influence environmental performance and nutrient retention [18]. Complementary agronomic studies show that fertilization systems can significantly affect soil agrochemical indicators and crop productivity, whether in cabbage or sweet potato, reinforcing that physical and chemical soil states are co-determining factors for water and nutrient acquisition [19,20].

Vineyards represent a particularly demanding case for soil physical quality and hydraulic functioning because they are perennial systems exposed to repeated traffic, often under slope conditions and in climates with high evaporative demand. Soil erosion and structural degradation in semi-arid vineyards have been documented under shallow tillage regimes, indicating that conventional operations can accelerate soil loss and degrade functional porosity [21]. At the same time, combined strategies such as organic mulching and no-tillage have demonstrated benefits for soil management under different water regimes, suggesting that reducing disturbance while protecting the surface can improve vineyard soil performance [22]. The broader success of strip tillage in improving productivity within rotational systems supports the relevance of localized tillage concepts, although most evidence has focused on annual crops and differs in root-zone geometry and traffic patterns from vineyards [23]. In this context, instrumentation and control systems for monitoring and precise control of tillage depth are increasingly relevant, because depth stability directly affects both the extent of compaction alleviation and the distribution of hydraulic improvements within the profile [24]. Optimization and testing methodologies for implement stability and operational performance in variable field conditions provide further tools for ensuring consistent depth and controlled disturbance, which are essential when the goal is hydrologically meaningful soil restoration rather than only surface tilth [25].

In parallel, the efficiency of deep loosening elements has been evaluated using rational utilization concepts that relate operating efficiency to how effectively mechanical input produces structural improvement, which is particularly useful when improved hydraulic functioning and root-zone water availability are primary management targets [26]. More unconventional approaches, such as pulse-type gas explosion subsoilers, also illustrate that “parameter optimization + field testing” can be framed explicitly in terms of soil physical change and functional outcomes, not only in terms of machine metrics

[27]. Likewise, performance evaluation of biomimetic rotary blades for straw incorporation indicates that design choices can significantly shape residue–soil mixing and aggregate response, with downstream consequences for infiltration and evaporation control [28]. Even when the crop system differs, these lines of work collectively underscore that sustainable tillage design must be evaluated through soil functional indicators that directly relate to water movement and root-zone behavior.

Beyond mechanization per se, broader sustainability studies show that cropping strategies influence root distribution and soil CO_2 emissions, linking soil structural conditions to carbon dynamics and ecosystem functioning [29]. Soil and water conservation measures on hillslopes have been assessed for effectiveness and suitability, reinforcing that hydrological context and slope processes must be considered when designing soil interventions in erosion-prone regions [30]. Experimental results from Hungary illustrate that tillage methods can alter soil moisture content and crop yield, again highlighting the direct pathway from mechanical disturbance to water availability and agronomic performance [31]. Technical work on experimental field installations for soil processing provides an operational basis for obtaining reliable traction and soil response data under controlled field conditions, which is necessary for defensible conclusions about soil restoration and hydrological improvement [32]. Closely related studies on movement stability of machine sections further show that accurate tool trajectory and depth maintenance are prerequisites for reproducible soil physical effects, especially in heterogeneous fields [33]. Fundamental analyses of rotor transporting ability in loosening and separating vehicles emphasize that material flow and soil conveyance are not merely mechanical details but factors that affect clod breakup patterns and post-tillage structural states relevant to infiltration [34]. Experimental studies of root crop choppers similarly highlight that field-validated assessment of working organ performance is indispensable when claiming functional improvements in soil–plant systems [35].

The rapid expansion of sensing, diagnostics, and data-driven control in agricultural machinery creates additional opportunities for maintaining stable tillage quality and preventing component wear that can degrade soil outcomes. For instance, lightweight detection algorithms for surface defects in small bearings illustrate how real-time diagnostics can support machinery reliability and consistent operation, which is directly relevant for sustained field performance of tillage equipment [36]. Standardized test procedures remain essential for comparing results and ensuring reproducibility across studies; in tillage engineering, ISO guidance provides a framework for reporting and evaluating soil-working equipment performance under defined conditions [37].

Within viticulture specifically, recent syntheses emphasize that soil management strategies must balance productivity with long-term soil quality, erosion control, and water conservation, with particular attention to compaction and hydraulic limitations in modern vineyards [38]. Cover cropping with legume-enriched mixtures can improve grape yield and quality in hillside vineyards, indicating that biological approaches can support soil function, yet they may not fully address deep mechanical impedance [39]. Selection of inter-row herbaceous covers in sloping, non-irrigated vineyards further demonstrates how vegetation management shapes erosion resistance and water dynamics, but also highlights that traffic and operational constraints remain influential [40]. The sustainability of machinery traffic in vineyards has been analyzed as a core determinant of soil compaction risk, reinforcing the need for traffic-compatible, localized interventions [41]. Integrated approaches for managing soil threats in vineyard ecosystems show that compaction and erosion often co-occur and must be handled in combination, with explicit attention to hydrological consequences [42]. Vineyard-focused studies also document that tillage-induced impacts affect soil properties, erosion, and nutrient loss, motivating management strategies that limit disturbance while restoring subsoil function

[43]. Soil carbon budget analyses in Mediterranean vineyards confirm that soil management can shift carbon trajectories, linking physical conservation to climate-related sustainability goals [44]. Targeted chisels for vineyards have been proposed, but the engineering challenge remains to design tools that loosen the compacted root strip effectively while minimizing inter-row disturbance and energy demand [45]. Additional work on organic mulches and under-vine management confirms that protecting the surface can reduce erosion and improve soil conditions, but mechanical intervention may still be necessary where compaction persists [46]. Studies on improving organic grape production also underscore that soil management and organic fertilization jointly influence productivity, supporting the view that structural restoration should be integrated with broader sustainability-oriented practices [47].

In many vineyard soils, the most restrictive mechanical impedance for grapevine roots occurs in the subsurface horizon formed by repeated machinery traffic and historical tillage operations. Field observations in compacted loam and serozem soils indicate that the zone between approximately 20 and 40 cm depth frequently coincides with the upper boundary of the traffic-induced compacted layer and the main zone of fine root elongation for grapevines.

Penetration resistance values exceeding 2–3 MPa within this horizon are commonly associated with restricted root growth and reduced hydraulic conductivity of the soil profile. The effectiveness of localized deep loosening in vineyards should also be interpreted within the broader framework of machinery traffic management. Repeated tractor passages are one of the principal drivers of subsoil compaction in perennial cropping systems, particularly in vineyards where spraying, canopy management, and harvesting operations occur several times during the growing season [12,41]. Consequently, the structural improvements achieved through localized strip tillage may gradually decline if subsequent machinery traffic occurs directly over the treated strip. From this perspective, the proposed U-shaped strip tillage tool should be integrated with traffic-restricted soil management strategies in which wheel tracks are preferentially confined to permanent inter-row lanes. Such an approach corresponds with modern vineyard soil management concepts that combine mechanical soil restoration with erosion control and long-term soil conservation strategies [38,42,43]. Consequently, mechanical loosening targeted specifically within the 20–40 cm layer can be expected to improve soil structural conditions relevant for root penetration and water movement without disturbing the entire soil profile.

Against this background, a clear knowledge gap persists: there is still limited, quantitatively validated evidence connecting geometry-optimized, strip-localized loosening tools in vineyards with hydrologically meaningful improvements in the root zone, such as increased infiltration and enhanced water availability under arid conditions, while maintaining moderate draft requirements and limiting surface disturbance.

The selection of the 20–40 cm soil layer as the target zone for mechanical intervention was based on the measured compaction profile of the experimental field and on published observations of grapevine rooting behaviour in comparable soils. Previous studies indicate that fine grapevine roots are often concentrated within the upper 40–60 cm of the soil profile, while traffic-induced compaction layers frequently develop between 20 and 40 cm depth. In the studied vineyard, penetration resistance measurements confirmed the presence of a mechanically restrictive layer beginning near 20 cm depth. Consequently, loosening within this horizon was considered the most effective strategy for alleviating mechanical impedance to root elongation and improving hydraulic continuity within the functional root zone.

Accordingly, the present study develops and evaluates a geometry-optimized U-shaped strip-tillage chisel designed for vineyard root-zone loosening. The approach

integrates theoretical substantiation, multifactor field experimentation, and the analysis of soil physical and hydrological indicators. It was hypothesized that the proposed working body configuration, when applied under compacted vineyard inter-row conditions, would be associated with reduced penetration resistance and bulk density, as well as increased infiltration capacity within the treated 20–40 cm soil layer relative to untreated compacted conditions and alternative tool configurations. This framework links engineering design with measurable soil physical responses relevant to sustainable vineyard management under semi-arid conditions.

2. Materials and Methods

2.1. Experimental Site and Soil Conditions

The experimental investigations were carried out in 2023–2024 at the experimental farm of the Bukhara Institute of Water Resources Management, affiliated with the National Research University "Tashkent Institute of Irrigation and Agricultural Mechanisation Engineers", Uzbekistan. The region belongs to a subtropical desert zone with a sharply continental, extremely arid climate. Summers are hot and dry, relative humidity is low, and sunshine duration exceeds 300 days annually, with mean daily temperatures during the growing season frequently surpassing 30 °C.

The predominant soil is light serozem of medium loam texture. Although serozem soils are representative for large areas of Central Asian viticulture, their structural and mechanical behaviour differs from that of heavy clay, gravelly, or highly calcareous vineyard soils commonly found in Mediterranean regions. Soil fracture propagation, draft resistance, and aggregate fragmentation may therefore respond differently to tool geometry under contrasting textural conditions [13,31]. Consequently, the results of the present study should be interpreted primarily within the context of medium-loam serozem soils, and additional validation experiments would be required to confirm the robustness of the optimized working body geometry across other vineyard soil types. To characterise baseline conditions prior to field trials, soil samples were collected along the diagonal transect of the experimental plot at five representative points. Undisturbed cores were taken from successive depth layers down to 20 cm for the determination of bulk density, while complementary subsamples were used for gravimetric moisture analysis. In situ penetration resistance profiling was performed to 45 cm depth in order to quantify the degree of compaction within the root zone. Initial measurements confirmed a gradual increase in soil strength and density with depth: penetration resistance values rose from approximately 1.2 MPa in the 0–10 cm layer to over 2.3 MPa below 20 cm, while bulk density increased from 1.24 g·cm^{-3} to 1.33 g·cm^{-3}. Gravimetric moisture content ranged between 9.7% and 12.6% across the measured horizons, reflecting the prevailing arid conditions.

These baseline data provided reference values for subsequent evaluation of tool performance in terms of soil loosening efficiency, aggregate size distribution, and improvements in root-zone hydrological properties.

All measurements were performed using five independent field replicates distributed across the experimental plot. For each physical indicator (penetration resistance, bulk density, and infiltration rate), the reported values represent arithmetic means calculated from replicated measurements. Data variability is expressed as standard deviation (mean ± SD).

2.2. Tool Design and Working Principle

A prototype strip tillage implement for vineyard root zone loosening was developed, consisting of a rigid frame, a three-point hitch attachment, depth-control wheels,

and a staple-shaped (U-form) working body (Figures 1–3). The frame (1) provides structural support for the working body and is connected to the tractor via a standard three-point hitch assembly (2). Adjustable gauge wheels (3) are mounted laterally to maintain consistent working depth across uneven terrain.

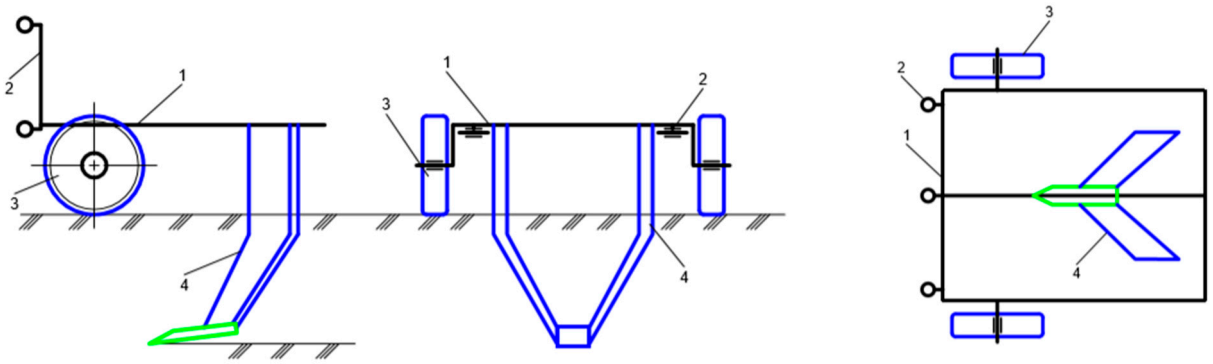


Figure 1. Schematic of the strip tillage implement: 1—frame; 2—three-point hitch; 3—gauge wheels; 4—U-shaped working body.

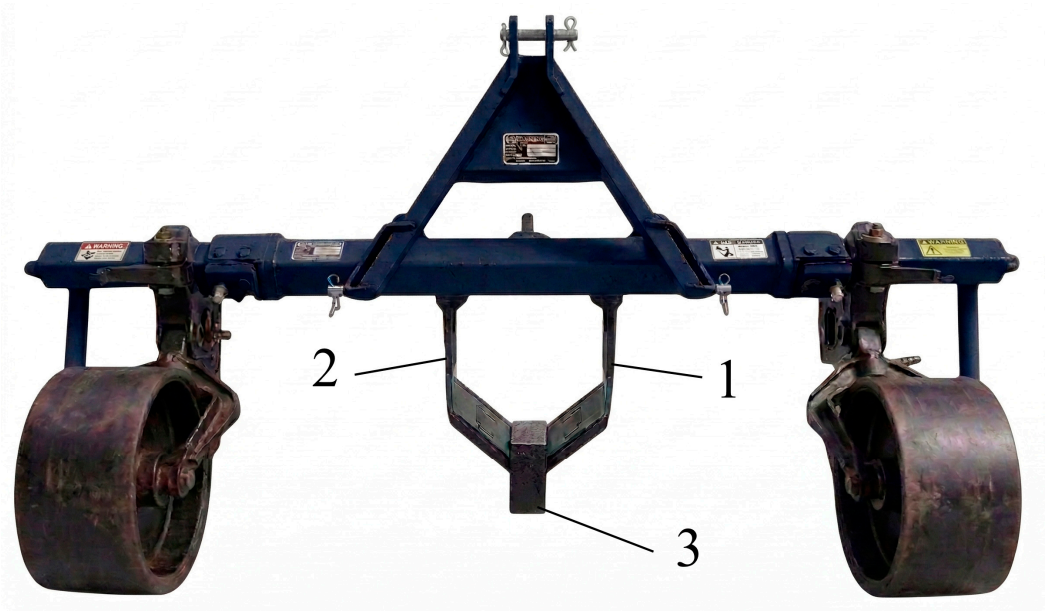


Figure 2. General view of the working body: 1—left shank; 2—right shank; 3—chisel.

The working body (4) comprises two inclined shanks positioned opposite each other and connected by a central chisel. The left (1) and right (2) shanks are mirror-symmetrical, with working surfaces oriented towards each other to confine and direct soil flow into the central loosening zone. The chisel (4) is mounted centrally between the shanks, its cutting edge inclined to the horizontal at 27–32°, as determined through theoretical analysis.

During operation, the chisel penetrates the compacted layer within the target strip, initiating crack formation in both longitudinal and transverse planes. The inclined sections of the shanks then enter these pre-formed cracks, lifting and bending the soil upwards along their working surfaces. This combined tensile and bending action intensifies aggregate breakdown, producing a high proportion of soil fragments smaller than 50 mm in diameter while limiting disturbance outside the strip.

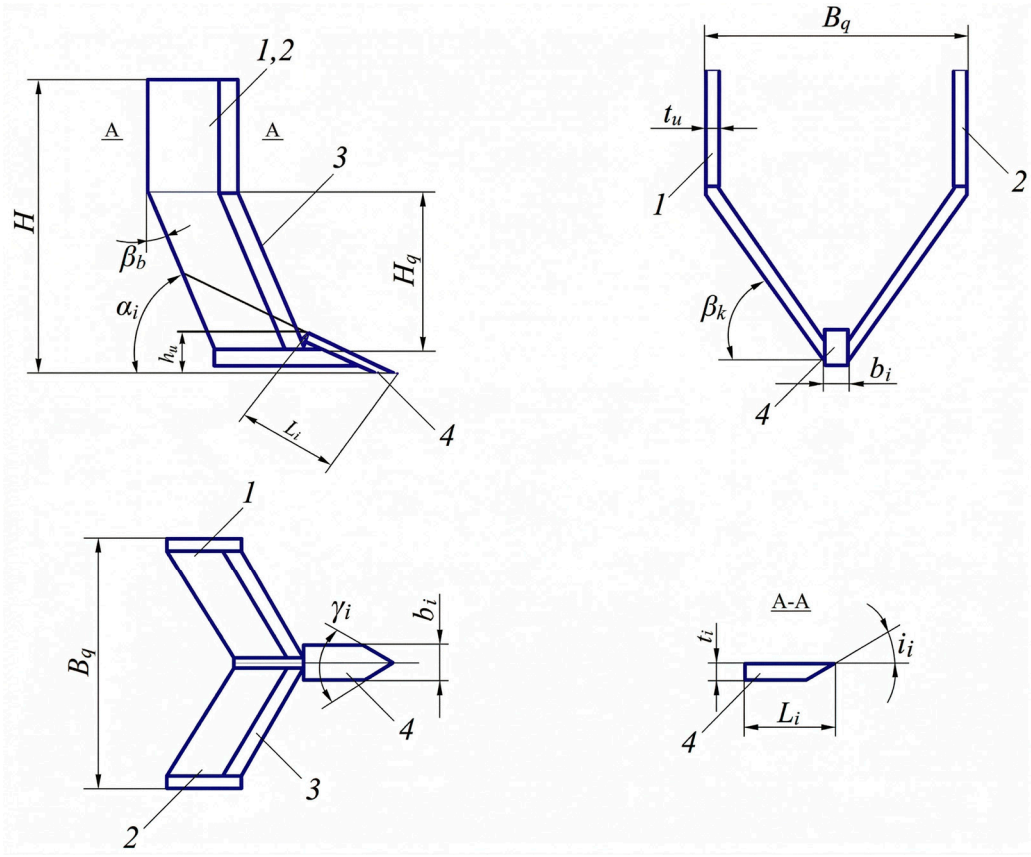


Figure 3. Main geometric parameters of the working body: 1—left shank; 2—right shank; 3—central stiffener (support bracket); 4—chisel.

Key geometric parameters affecting tool performance include shank height, inclination angles in both longitudinal–vertical and transverse–vertical planes, spacing between shanks, chisel width and length, and chisel entry angle. In the developed design, the shank height is 0.70 m, with the inclined section measuring 0.30 m. The minimum transverse distance between shanks is 0.62 m, while the chisel width and length are 0.11 m and 0.27 m, respectively. The shanks are inclined at 20° in the longitudinal–vertical plane and 40–45° in the transverse–vertical plane.

2.3. Theoretical Calculations

The geometric configuration of the working body was developed based on theoretical assumptions of soil fracture mechanics, structural geometry, and energy-efficient design. All variables correspond to the notations defined in Figure 3.

The total height H of the shank was derived to ensure sufficient clearance for loosened soil and crop residues under the machine frame:

$$H = h_1 + h_2 + a \quad (1)$$

where h_1 is the clearance between the frame and the loosened soil surface (m), h_2 is the maximum ridge height of loosened soil (m), and a is the working depth (m).

Using $h_1 = 0.30$ m, $h_2 = 0.075$ m, and $a = 0.30$ m, the total height is $H = 0.675$ m ≈ 0.70 m.

To ensure effective cutting of soil and plant residues, the longitudinal inclination angle β_b must satisfy:

$$0 < \beta_b < \varphi \quad (2)$$

where φ is the soil–metal friction angle (typically 25°). The optimal value is $\beta_b = 20°$.

The transverse inclination angle β_k is assumed to be equal to the soil shear fracture angle ψ_k, giving

$$\beta_k = \psi_k = 45^\circ \tag{3}$$

The maximum permissible length of the chisel L_i was determined from soil fracture theory according to the relation:

$$L \le \frac{2a\left(I + \frac{T_e}{\rho g a}\right)\cos\varphi\sin(\alpha+\varphi)}{q_0 \cos\left(\alpha + \frac{\varphi_1}{2}\right)} \tag{4}$$

where T_e—specific soil compression resistance (Pa); ρ—soil density (kg·m^{-3}); g—gravitational acceleration (9.81 m·s^{-2}); q_0, I—empirical coefficients; φ, φ_1—soil friction angles; α—the angle between the cutting edge (working face of the chisel) and the horizontal plane.

From the analysis: $Li \le 0.27$ m.

The chisel entry angle α_i, important for minimizing resistance, is calculated as:

$$\alpha_i = \arctan\left(-\tan\varphi + \sqrt{\tan^2\varphi + 1}\right) \tag{5}$$

Assuming φ = 25–30°, the recommended value is α_i = 27.5–31.5°.

To ensure proper depth and crack formation, the minimum width bi is calculated from:

$$b_i \ge \frac{(4.2 + \cot(\alpha_i))a(a - (h_{ib} + h_b))T_e}{0.1\tau(3\varepsilon - 1.5)} \tag{6}$$

where τ—soil shear resistance (Pa); ε—deformation coefficient; h_{ib}—distance from chisel tip to base (m); h_b—boss height (m).

Computed value: $b_i \ge 0.11$ m.

The total height of the shank was adopted as H = 0.70 m, with the inclined section of the shank set to H_q = 0.30 m. The working depth of the tool was a = 0.30 m, while the required clearance between the frame and the loosened soil surface was h_1 = 0.30 m. The ridge height of loosened soil above the original ground level was taken as h_2 = 0.075 m.

The inclination angles of the shank in the longitudinal and transverse vertical planes were defined as β_b = 20° and β_k = 45°, respectively. The chisel entry angle ranged from α_i = 27.5° to 31.5°, and the bevel angle at the A–A section was assumed approximately equal to this value.

The spacing between the inclined shanks was defined in the range B_q = 0.62–0.64 m. The minimum width of the chisel was calculated to b_e $b_i \ge 0.11$ m, and the maximum length was $L_i \le 0.27$ m, ensuring efficient crack propagation.

The thickness of the chisel at section A–A was taken as ti = 8 mm, and the wall thickness of the upper part of the frame was adopted as t_u = 5 mm. Finally, the divergence angle between the two shanks in the horizontal projection was in the range γ_i = 85–95°.

2.4. Experimental Setup

The experimental programme was carried out using a specially developed laboratory–field unit designed to evaluate the performance of alternative tillage working bodies under both controlled and operational conditions. The unit was constructed as a rigid welded steel frame equipped with a standard three-point hitch for tractor mounting. A central carriage allowed rapid replacement of working bodies, including the prototype

U-shaped strip tillage implement, inclined shank "paraplow" elements, and chisels of different widths and lengths. Such modularity ensured that all treatments were tested at identical working depths, forward speeds, and soil conditions, thereby enabling strict comparability of results (Figure 4).

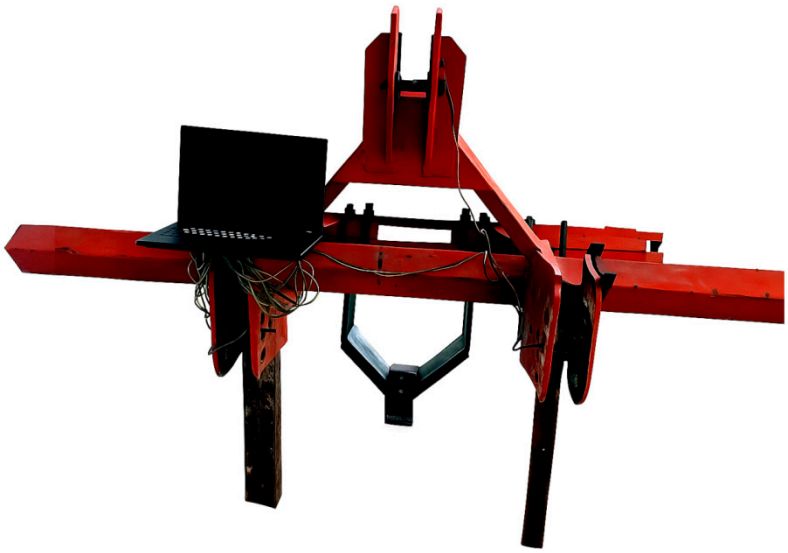


Figure 4. General view of the laboratory–field experimental unit with the mounted working body, showing the rigid frame, tool carriage, and mounting configuration for the prototype implement.

The primary performance indicators selected for evaluation were: (i) draft force (kN); (ii) soil crushing degree expressed as the proportion of clods smaller than 50 mm ($F_{<50}$, %); (iii) soil penetration resistance (PR, MPa); (iv) bulk density (ρ, g·cm^{-3}); and (v) infiltration rate (mm·h^{-1}). These complementary parameters were chosen to provide a comprehensive assessment of both mechanical energy efficiency and the capacity of the tool to improve root-zone physical conditions.

Draft force was measured using strain-gauge-based force transducers (tensometric pins, HBM GmbH, Darmstadt, Germany) integrated directly into the tractor's three-point hitch. Sensors were positioned on both the upper and lower linkages to capture the full load spectrum. The upper sensors recorded tensile forces in the top link, while the lower sensors measured compressive and bending forces in the lift arms, enabling simultaneous monitoring of horizontal draft and vertical reactions during operation (Figure 5).



Figure 5. Position of the tensometric pins installed on the tractor three-point hitch, showing the integration with the upper top link and the lower lift arms.

Signals from all sensors were transmitted to a portable data acquisition system (QuantumX MX840A, HBM GmbH, Darmstadt, Germany) connected to a laptop computer (Lenovo ThinkPad E14, Lenovo Group Ltd., Beijing, China), allowing real-time recording and monitoring of force dynamics during tillage. Calibration of the measurement system was carried out before and after each test series using certified static loads, ensuring accuracy within ±0.5%. Detailed views of the tensometric pin sensors are provided in Figure 6.



(**a**) (**b**)

Figure 6. Detailed view of the tensometric pin sensors: (**a**) upper sensors used for measuring tensile loads in the top link; (**b**) lower sensors used for measuring compressive and bending loads in the lift arms.

Immediately after each tillage pass, disturbed soil samples were collected from the centre of the cultivated strip for aggregate size analysis. Crushing efficiency ($F_{<50}$, %) was quantified as the proportion of soil aggregates smaller than 50 mm relative to the total dry mass, determined using a standard sieve set (Endecotts Ltd., London, UK). The fragmentation index $F_{<50}$ was used primarily as an engineering indicator of soil-crushing efficiency rather than as a direct agronomic indicator of root growth conditions. This index reflects the ability of the working body to disrupt compacted aggregates and initiate fracture propagation within the disturbed strip. Increased fragmentation promotes the formation of macropores and reduces mechanical impedance, thereby indirectly supporting root penetration and water movement. Although the threshold value of 50 mm originates from standardized tillage evaluation procedures, in the present study it serves as a comparative indicator allowing different working body geometries to be evaluated under equivalent experimental conditions. This parameter served as the primary indicator of soil loosening efficiency within the cultivated strip.

In addition, field measurements of soil penetration resistance were conducted in situ adjacent to the tilled strips using a GPS-equipped cone penetrometer to a depth of 45 cm. These data were used to characterise the extent of subsoil compaction relief within the vineyard root zone. Bulk density was determined from undisturbed soil cores (Eijkelkamp Soil & Water, Giesbeek, Netherlands) collected after tillage, enabling evaluation of changes in porosity and soil structure in the 20–40 cm layer. Infiltration rate was measured with a double-ring infiltrometer placed within the tilled strip to quantify improvements in water intake capacity following treatment. Together, these measurements provided an integrated basis for validating the tool's ability to reduce soil strength, alle-

viate compaction, and enhance hydrological conditions while limiting surface disturbance in vineyard inter-rows.

2.5. Experimental Design

The research programme was structured using both one-factor and multifactor experimental designs to investigate the influence of key operational and geometric parameters of the strip tillage working body on soil-crushing efficiency, draft force, and soil physical responses. The experimental matrix was developed in accordance with standard agricultural engineering methodology for process optimisation, enabling the identification of both individual and interaction effects of the selected factors.

In the one-factor plan, each parameter was varied independently while the others were held constant at their nominal levels. This allowed for a preliminary assessment of the magnitude and direction of each factor's effect on the measured responses. In the multifactor plan, a full factorial scheme was implemented, enabling the simultaneous variation of all factors across defined levels. This approach allowed for the analysis of factor interactions and the development of empirical regression models to predict performance indicators within the studied parameter space.

The following four independent variables (factors) were selected: X_1—chisel working depth, a (cm); X_2—chisel width, bi (cm); X_3—forward speed of the tractor–implement system, V (km·h^{-1}); X_4—rake angle of the inclined shank, β_β (degrees). The ranges and levels for each factor were determined based on preliminary trials, theoretical calculations (Section 2.3), and operational constraints of the tractor–implement system. The factor ranges are presented in Table 1. The lower, central, and upper levels were coded as −1, 0, and +1, respectively, to facilitate statistical analysis.

Table 1. Experimental factors, designations, physical ranges, and coded levels for the full factorial design.

Factor Code	Factor Description	Unit	Lower Level (−1)	Central Level (0)	Upper Level (+1)
X_1	Chisel working depth (a)	cm	20	25	30
X_2	Chisel width (bi)	cm	9	11	13
X_3	Forward speed of tractor–implement system	km·h^{-1}	4	5	6
X_4	Rake angle of inclined shank (β)	degrees	15	20	25

In this experimental design, X_1 and X_2 represented the primary geometric parameters of the working body that directly influence the depth of soil penetration and the cross-sectional area of soil engagement, thereby affecting soil loosening and aggregate breakdown. X_3 reflected the operational speed, which impacts both energy input and dynamic soil–tool interaction. X_4 defined the inclination of the shank relative to the vertical plane, influencing the cutting mechanism, soil disturbance pattern, and draft requirements.

The ranges were selected based on theoretical optimisation criteria (Section 2.3) and preliminary operational trials. The lower and upper limits ensured safe operation of the implement without excessive draft force, while the central levels corresponded to the baseline configuration recommended for vineyard strip tillage under Uzbekistan's soil conditions.

To ensure accuracy, reliability, and reproducibility, all tests were performed in triplicate. Outliers were identified and excluded using the Grubbs test at a significance level of $p = 0.05$. Homogeneity of variance was assessed by the Cochran criterion (Equation (7)). The significance of regression coefficients was verified by the Student t-test (Equation (8)), and model adequacy was confirmed using the Fisher criterion (Equation (9)).

Statistical analyses, including ANOVA, regression modelling, and adequacy testing, were performed using Statistica 13.3 (TIBCO Software Inc., Palo Alto, CA, USA).

The soil-crushing degree ($F_{<50}$, %) was determined as the dry mass fraction of aggregates smaller than 50 mm relative to the total sample (Equation (10)). In addition, field measurements of penetration resistance (PR, MPa), bulk density (ρ, g·cm^{-3}), and infiltration rate (mm·h^{-1}) were integrated into the experimental plan to validate tool performance in terms of root-zone compaction relief and hydrological improvement. Together, these indicators provided a comprehensive validation of the hypothesised advantages of the prototype strip tillage implement.

To ensure strict comparability of the experimental treatments, all working bodies were operated under identical field conditions, including the same working depth, tractor power class, forward speed, soil moisture conditions, and soil texture. The interchangeable mounting system of the laboratory–field unit allowed the tested working bodies to be installed on the same frame without altering the operational configuration of the machine.

$$G = \frac{max(S_i^2)}{\sum_{i=1}^{k} S_i^2} \tag{7}$$

where S_i is the variance of the i-th treatment group, and k is the number of groups. Homogeneity was assumed if $G \le G_{tab}(p = 0.05, k, n)$. This criterion was applied separately to replicate data for $F_{<50}$, draft force, PR, bulk density, and infiltration rate.

$$t_i = \frac{b_i}{S_{b_i}} \tag{8}$$

where b_i is the estimated regression coefficient for factor X_i, and S_{bi} is its standard error. Coefficients were considered statistically significant if $|t_i| \ge t_{tab}(p = 0.05, f)$, where f is the number of degrees of freedom. This test allowed identification of the most influential factors for all measured responses.

$$F = \frac{S^2_{\text{model}}}{S^2_{\text{residual}}} = \frac{\sum_{j=1}^{m} (\hat{y}_j - \overline{y})^2 / f_1}{\sum_{j=1}^{m} (y_j - \hat{y}_j)^2 / f_2} \tag{9}$$

where $\hat{y}_j$ is the predicted response, y_j is the observed response, $\overline{y}$ is the mean value, S^2_{model} is the explained variance, and S^2_{residual} is the residual variance. Degrees of freedom are $f_1 = m - p$ and $f_2 = m - p - 1$, where m is the number of experiments and p is the number of regression coefficients. Adequacy was confirmed when $F \le F_{tab}$ ($p = 0.05, f_1, f_2$).

$$F_{<50} = \frac{m_{<50}}{m_{total}} \times 100 \tag{10}$$

where $m_{<50}$ is the dry mass of soil aggregates smaller than 50 mm, and m_{total} is the total dry mass of the sample. This index quantified the effectiveness of aggregate breakdown by the working body. Higher values of $F_{<50}$ corresponded to improved loosening and were further correlated with reductions in PR and ρ, as well as increases in infiltration rate.

The present experimental design does not allow the separation of the effects of working body geometry from the total mechanical energy input on soil structural response. Although draft force and operational parameters were measured and controlled,

modifications in tool geometry inherently altered the distribution of mechanical energy within the soil. Therefore, the observed changes in soil fragmentation, penetration resistance, bulk density, and infiltration rate should be interpreted as resulting from the combined effect of geometry optimisation and associated energy transfer, rather than from geometry alone in a strictly causal sense.

2.6. Soil Measurements and Standards

Soil physical and hydrological parameters were measured in accordance with internationally recognised standards to ensure comparability and reproducibility of results. Bulk density (ρ, g·cm^{-3}) was determined on undisturbed soil cores with a volume of 503 cm^3 following *ISO 11272:2017 Soil quality—Determination of dry bulk density*. Gravimetric soil water content was measured on subsamples according to *ISO 11465:1993 Soil quality—Determination of dry matter and water content on a mass basis*.

Soil penetration resistance (PR, MPa) was measured in situ using a handheld GPS cone penetrometer (Datafield, Kyiv, Ukraine) equipped with a polished steel cone of 30° apex angle and 20.27 mm base diameter. For heavy clay loam soils, a smaller cone of 12.83 mm (½″) was used. The procedure followed the *ASABE Standard EP542: Procedures for Using and Reporting Data Obtained with the Soil Cone Penetrometer*, with measurements taken at a quasi-static penetration rate of 30 mm·s^{-1}. Profiles were recorded to a depth of 45 cm and georeferenced via the integrated GPS module. For graphical presentation of penetration resistance profiles in several figures, the original scale of the cone penetrometer was retained in kg·cm^{-2}, which corresponds to the instrument calibration used during field measurements. For clarity and consistency with the SI system, all analytical calculations and statistical analyses were performed using penetration resistance values expressed in MPa. The conversion factor used was 1 kg·cm^{-2} = 0.098 MPa.

The degree of soil crushing was quantified as the fraction of aggregates smaller than 50 mm ($F_{<50}$, %) relative to the total dry mass, determined according to *ISO 7256/1:1984 Agricultural requirements and test procedures for disc harrows* and complemented by the sieve method specified in *ISO 11277:2020 Soil quality—Determination of particle size distribution in mineral soil material*.

Infiltration rate (mm·h^{-1}) was measured in the field using a double-ring infiltrometer following ASTM D3385-18 Standard Test Method for Infiltration Rate of Soils in Field Using Double-Ring Infiltrometer and ISO 17312:2005 Soil quality—Determination of the rate of water infiltration in soil. Measurements were conducted within the cultivated strip immediately after tillage to capture the effect of loosening on root-zone hydrological properties.

All experimental data were subjected to statistical analysis, including ANOVA, regression modelling, and adequacy testing. Variance homogeneity was assessed using the Cochran criterion (Equation (7)), the significance of regression coefficients was tested with Student's *t*-test (Equation (8)), and model adequacy was confirmed using the Fisher criterion (Equation (9)). The soil-crushing degree was calculated according to Equation (10). Statistical terminology and reporting were aligned with *ISO 3534-1:2006 Statistics—Vocabulary and symbols—Part 1: General statistical terms and terms used in probability*. All analyses were performed using Statistica 13.3 (TIBCO Software Inc., Palo Alto, CA, USA). All reported quantitative data are presented as mean ± SD based on three independent replicates (n = 3), unless otherwise indicated.

3. Results

3.1. Single-Factor Experiments on Design Parameters Influencing Soil Fragmentation and Draft Resistance

A series of single-factor experiments was carried out to investigate the influence of key design parameters of the staple-shaped working body on soil-crushing efficiency and energy demand under vineyard root zone conditions. For comparative evaluation, three types of working bodies were tested: a conventional single paraplow-type inclined shank, a configuration with two opposing paraplow shanks, and the proposed U-shaped strip tillage working body. The geometric parameters of these working bodies are summarized in Table 2. This comparison allowed the effect of the optimized geometry to be evaluated relative to alternative soil-loosening configurations under equivalent operational conditions. The main indicators used for performance evaluation were the fraction of soil clods smaller than 50 mm in diameter ($F_{<50}$, %), hereafter referred to as soil-crushing efficiency, and the draft resistance (R, kN) measured at the tractor hitch point. Tests were conducted at forward speeds of 4 and 6 km·h^{-1} in compacted light serozem soil with a medium loam texture and a distinct plough pan layer. Unless otherwise stated, the plotted values represent mean ± SD obtained from three independent replicates (n = 3).

Table 2. Geometric parameters of the working bodies used in comparative experiments.

Working Body Type	Shank Inclination β_b (°)	Transverse Inclination β_k (°)	Chisel Width b_i (m)	Working Depth a (m)	Spacing Between Shanks B_q (m)
Single paraplow shank	20	40	0.11	0.30	–
Double paraplow shanks	20	40	0.11	0.30	0.62
U-shaped optimized strip tillage tool	20	40–45	0.11	0.30	0.62–0.64

The persistence of the observed structural improvements is closely related to the spatial distribution of machinery traffic within vineyard systems. In perennial crops such as vineyards, repeated operations including spraying, fertilization, and harvesting frequently occur along the same inter-row lanes [12,41]. If subsequent tractor passes occur directly over the loosened strip, the mechanical benefits of localized deep loosening may be progressively reduced due to rapid re-compaction of the soil [12]. Therefore, the effectiveness of strip-localized loosening can be substantially enhanced when combined with traffic-management strategies such as permanent traffic lanes or Controlled Traffic Farming (CTF) systems. Under such conditions, mechanical disturbance is confined to predefined wheel tracks while the treated root-zone strips remain largely protected from repeated compressive loading. Integrating geometry-optimized strip tillage with traffic management therefore represents a promising approach for maintaining long-term improvements in soil physical quality and hydraulic functioning in vineyard agroecosystems.

Serozem soils possess specific physical characteristics, including carbonate accumulation in the subsoil and relatively weak structural aggregation, which influence soil–tool interaction and fracture propagation during deep loosening. Consequently, the quantitative results obtained in this study should be interpreted within the context of this soil type. Although the mechanical principles underlying the proposed tool design are expected to remain valid across different soils, additional validation experiments on contrasting textures, including heavy clay soils, gravelly substrates and calcareous vineyard soils, would be required to confirm the robustness of the optimized geometry under broader field conditions.

The first stage involved comparing three types of working body designs: (i) a single paraplow-type inclined shank, (ii) a pair of paraplow-type inclined shanks with opposing working faces, and (iii) the proposed staple-shaped working body with two inclined shanks joined by a central chisel. The results (Figure 7) demonstrated that the staple-shaped working body achieved the most favourable combination of high soil-crushing efficiency and reduced draft resistance. Its geometry promoted controlled crack propagation within the target strip, effectively fragmenting soil aggregates while minimising disturbance beyond the root zone.

Following this, the effect of shank spacing (B_q) was assessed. As shown in Figure 8, increasing the spacing between side shanks from 0.50 m to 0.70 m caused a gradual reduction in $F_{<50}$, indicating less efficient soil breakdown. Draft resistance exhibited a concave-parabolic trend: it decreased initially as spacing increased (due to reduced soil–metal contact area and lower compaction between shanks), but beyond a certain point began to rise again, likely due to less synergistic soil fracture between the two shanks. Optimal performance, balancing high $F_{<50}$ with minimal R, was achieved at B_q values between 0.62 m and 0.64 m, which is below the 0.65 m threshold identified as critical for maintaining adequate crushing efficiency.

The influence of chisel width (b_i) was then investigated. The results (Figure 9) indicated that changes in bi from 0.05 m to 0.13 m had only a minor effect on soil-crushing efficiency, with $F_{<50}$ remaining relatively stable. However, draft resistance increased linearly with chisel width, as a wider chisel displaced a proportionally larger soil volume. Based on this, an optimal chisel width in the range of 0.10–0.12 m was recommended for the tested soil conditions.

The longitudinal–vertical inclination angle of the shanks (β_b) was also studied. Increasing β_b from 10° to 25° (Figure 10) resulted in a concave-parabolic rise in $F_{<50}$, with draft resistance initially decreasing before increasing again at higher angles. This pattern can be explained by the interaction between the shanks and the pre-formed cracks created by the chisel: at moderate inclinations (14–18°), the shanks most effectively penetrated and lifted the soil, enhancing aggregate breakdown while keeping draft forces low. Outside this range, either insufficient bending (at low β_b) or excessive compression (at high β_b) reduced overall performance. This optimal β_b range corresponded to an angle between the inclined parts of the left and right shanks (γ) of 85–95°.

The chisel entry angle (α) proved critical for balancing cutting efficiency with energy input. Experimental results confirmed that an α between 30° and 35° provided the best trade-off, yielding high $F_{<50}$ values (over 80%) while avoiding excessive draft forces or unnecessary soil disturbance.

Finally, the influence of shank width was evaluated (Figure 11). Increasing shank width from 0.05 m to 0.13 m expanded the deformation zone, which led to a higher proportion of large clods (>50 mm) and a linear increase in draft resistance. The explanation lies in the proportional relationship between shank width and the volume of soil subjected to direct deformation. Wider shanks mobilise more soil, requiring greater energy and producing larger aggregates. A shank width of 0.10–0.12 m was therefore found to be optimal.

Overall, the single-factor experimental results clearly indicated that the staple-shaped working body delivers the best performance when configured with a shank spacing (B_q) of 0.62–0.64 m, chisel width (b_i) of 0.11 m, longitudinal–vertical shank inclination (β_b) of 14–18°, chisel entry angle (α) of 30–35°, and shank width of 0.10–0.12 m. This configuration consistently achieved soil-crushing efficiency values above 80% ($F_{<50}$) while maintaining moderate draft resistance, thereby meeting the agronomic requirements for deep, strip-localised loosening in vineyard root zones under compacted arid-zone soil conditions.

https://doi.org/10.3390/agriculture16070751

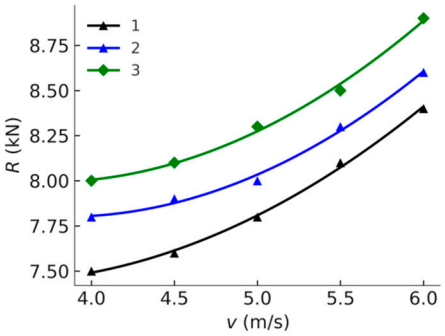


Figure 7. Variation in draft resistance (*R*) with working body design. 1—single paraplow shank; 2—double paraplow shanks with opposite faces; 3—staple-shaped working body. Values are presented as mean ± SD (n = 3).

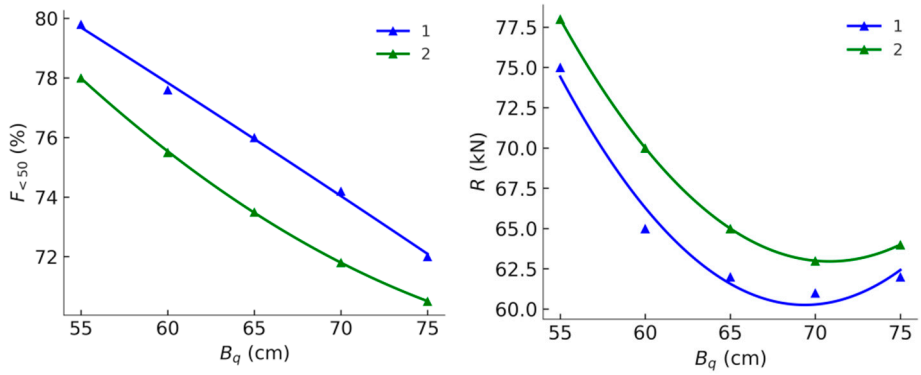


Figure 8. Variation in soil-crushing efficiency ($F_{<50}$) and draft resistance (*R*) with shank spacing (B_q) of the staple-shaped working body. 1—V = 4 km·h^{-1}; 2—V = 6 km·h^{-1}. Values are presented as mean ± SD (n = 3).

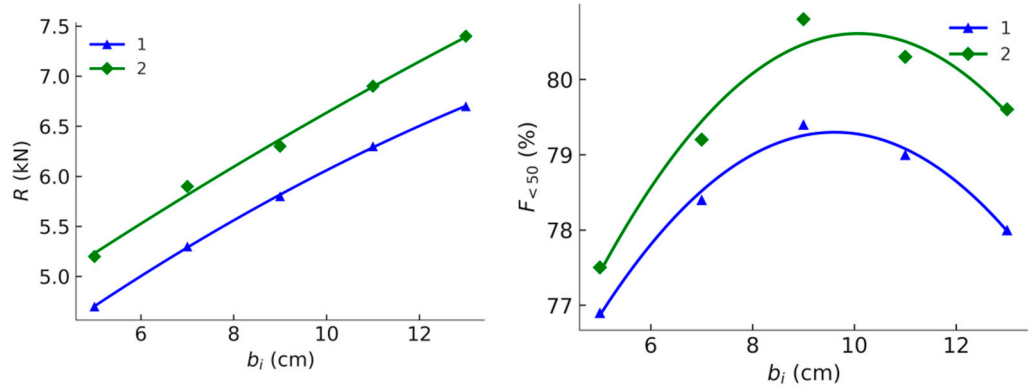


Figure 9. Variation in soil-crushing efficiency ($F_{<50}$) and draft resistance (*R*) with chisel width (b_i). 1—V = 4 km·h^{-1}; 2—V = 6 km·h^{-1}. Values are presented as mean ± SD (n = 3).

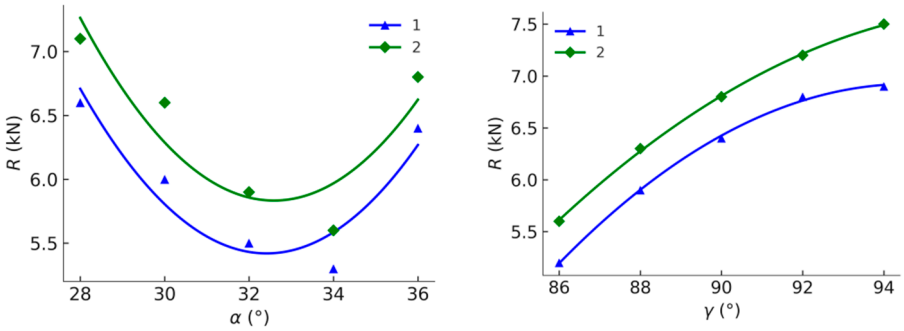


Figure 10. Variation in soil-crushing efficiency ($F_{<50}$) and draft resistance (R) with chisel entry angle (α). 1—V = 4 km·h^{-1}; 2—V = 6 km·h^{-1}. Values are presented as mean ± SD (n = 3).

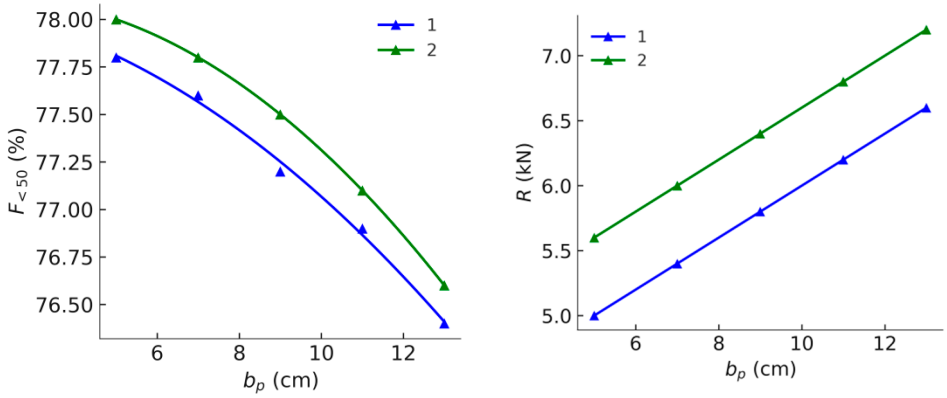


Figure 11. Variation in soil-crushing efficiency ($F_{<50}$) and draft resistance (R) with shank width. 1—V = 4 km·h^{-1}; 2—V = 6 km·h^{-1}. Values are presented as mean ± SD (n = 3).

3.2. Multifactor Regression Analysis and Response Surface Optimisation of Soil Fragmentation and Draft Resistance

Following the single-factor investigations, a multifactor experimental study was conducted to evaluate the combined effects of the most influential parameters on soil-crushing efficiency ($F_{<50}$) and draft resistance (R). The parameters selected from the results of Section 3.1 were: the angle between the inclined parts of the left and right shanks (γ, degrees), the chisel entry angle (α, degrees), the spacing between side shanks (B_q, m), and the forward travel speed of the aggregate (V, km·h^{-1}).

A central composite design was applied to plan the experiments, enabling the estimation of second-order polynomial regression models that describe the relationships between these parameters and the output responses. The general form of the regression equation for each response variable Y is expressed as:

$$Y = b_0 + b_1X_1 + b_2X_2 + b_3X_3 + b_4X_4 + b_{12}X_1X_2 + b_{13}X_1X_3 + b_{14}X_1X_4 + b_{23}X_2X_3 + b_{24}X_2X_4 + b_{34}X_3X_4 + b_{11}X_1^2 + b_{22}X_2^2 + b_{33}X_3^2 + b_{44}X_4^2 \quad (11)$$

where $X_1 = \gamma$—angle between inclined shanks (°); $X_2 = \alpha$—chisel entry angle (°); $X_3 = B_q$—shank spacing (m); $X_4 = V$—forward travel speed (km·h^{-1})

For soil-crushing efficiency ($F_{<50}$), the regression model derived from the analysis of variance was:

$$F_{<50} = 82.14 + 1.26X_1 + 0.94X_2 - 2.31X_3 + 1.57X_4 + 0.68X_1X_2 - 0.54X_1X_3 + 0.42X_2X_3 - 0.39X_3X_4 - 1.18X_1^2 - 0.97X_2^2 - 0.84X_3^2 - 0.65X_4^2 \quad (12)$$

The coefficient of determination for Equation (12) was $R^2 = 0.94$, indicating that the model explained 94% of the variability in the experimental data. The positive coefficients for X_1 and X_2 confirm that moderate increases in the shank inclination angle and chisel

entry angle improve soil breakdown, while the negative coefficients for X_3 and the quadratic terms show that excessive increases in shank spacing or other factors reduce crushing efficiency.

For draft resistance (R), the regression equation was:

$$R = 4.92 + 0.083X_1 + 0.056X_2 + 0.49X_3 + 0.61X_4 + 0.034X_1X_3 + 0.028X_2X_4 + 0.021X_3X_4 + 0.041X_1^2 + 0.037X_2^2 + 0.054X_3^2 + 0.045X_4^2 \quad (13)$$

The draft resistance model achieved $R^2 = 0.92$, confirming its high predictive capability. The positive coefficients for X_3 and X_4 indicate that increasing shank spacing and operating speed both raise the energy demand, while the quadratic terms suggest that the effect intensifies beyond optimal settings.

Response surface plots generated from Equations (12) and (13) (Figures 12–14) illustrate the interactions between the parameters. For example, Figure 12 (Effect of γ and α on $F_{<50}$ at $B_q = 0.63$ m and $V = 5$ km·h^{-1}) shows that maximum crushing efficiency (>85%) occurs at γ values of 88–92° and α values of 32–34°. Figure 13 (Effect of B_q and V on R at $\gamma = 90°$ and $\alpha = 33°$) demonstrates that the lowest draft resistance is obtained at the lower limit of the optimal shank spacing range and moderate forward speeds (4–5 km·h^{-1}).

By applying a desirability function that targeted $F_{<50} \geq 80\%$ and $R \leq 5.0$ kN, the simultaneous optimisation of both regression models identified the optimal parameter combination as: $\gamma = 90°$; $\alpha = 33°$; $B_q = 0.63$ m; $V = 4.8$ km·h^{-1}.

Under these conditions, the predicted responses were $F_{<50} = 84.9\%$ and $R = 4.87$ kN. Validation experiments based on three independent replicates confirmed these predictions within a ±3% deviation, demonstrating the robustness of the model.

Figure 12 illustrates the response surface of soil-crushing efficiency ($F_{<50}$) as a function of the angle between the inclined shanks (γ) and the chisel entry angle (α) under constant conditions of shank spacing $B_q = 0.63$ m and travel speed $V = 5$ km·h^{-1}. The plot shows that $F_{<50}$ varies within the range of approximately 72% to 85% across the studied factor levels. The maximum crushing efficiency, reaching 84–85%, is observed at intermediate values of γ between 88° and 92°, combined with α values in the range of 32–34°. At lower γ (85–86°) and α (28–29°), the efficiency drops to about 72–74%. Increasing γ beyond 94° or α above 35° leads to a gradual decline in $F_{<50}$ to around 76–78%, indicating the presence of an optimum zone rather than a strictly monotonic relationship. The surface curvature suggests significant interaction between γ and α, with the most favourable region forming a ridge that extends diagonally across the γ–α parameter space.

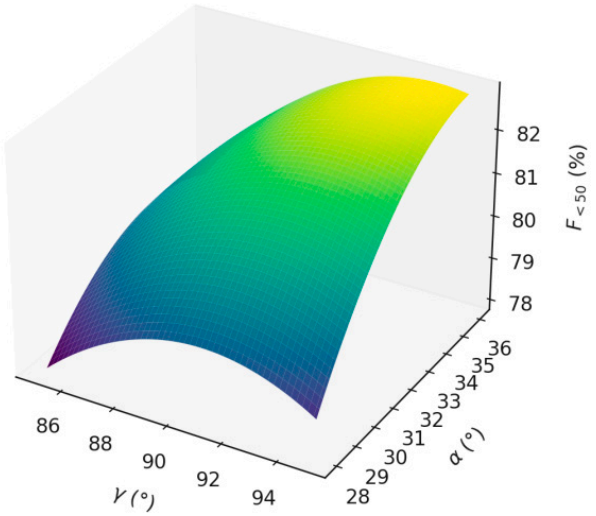


Figure 12. Response surface for soil-crushing efficiency ($F_{<50}$) as a function of γ and α at $B_q = 0.63$ m and $V = 5$ km·h^{-1}.

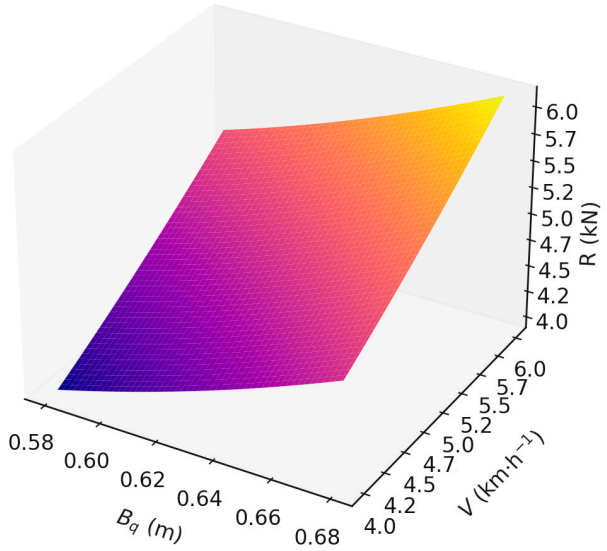


Figure 13. Effect of B_q (shank spacing) and V (travel speed) on draft resistance (R) at $\gamma = 90°$ and $\alpha = 33°$.

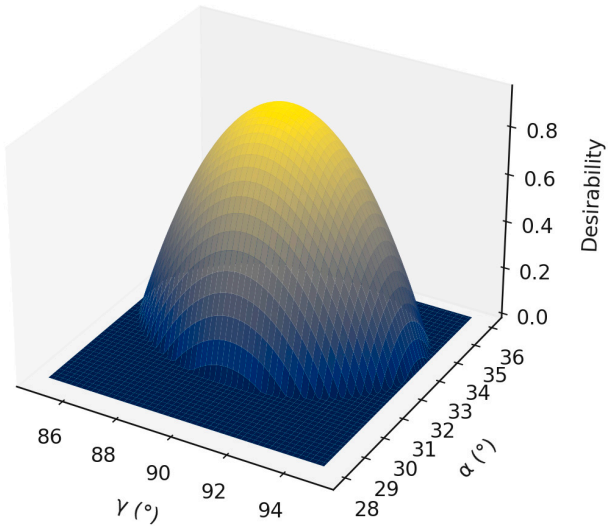


Figure 14. Response surface showing the combined desirability function for simultaneous optimisation of $F_{<50}$ and R.

Figure 13 shows Draft resistance (R) as a function of shank spacing (B_q) and travel speed (V) with fixed $\gamma = 90°$ and $\alpha = 33°$. The calculated draft resistance ranges from approximately 4.65 kN to 5.45 kN across the studied factor levels. The lowest resistance values, around 4.65–4.75 kN, occur at the smallest tested shank spacing ($Bq \approx 0.58$–0.60 m) combined with moderate travel speeds of 4.0–4.5 km·h^{-1}. As B_q increases beyond 0.65 m, R rises sharply, reaching 5.35–5.45 kN at the maximum tested spacing ($B_q = 0.68$ m). A similar, though less pronounced, effect is observed with increasing travel speed: raising V from 4.0 km·h^{-1} to 6.0 km·h^{-1} at constant B_q increases draft resistance by approximately 0.4–0.5 kN. The response surface shows a distinct valley along the low B_q and low-to-moderate V region, confirming that both parameters should be controlled jointly to minimise energy consumption during operation.

Figure 14 shows the combined desirability surface for simultaneous optimisation of soil-crushing efficiency ($F_{<50}$) and draft resistance (R) as a function of the angle between the inclined shanks (γ) and the chisel entry angle (α) at fixed shank spacing $Bq = 0.63$ m and travel speed $V = 5$ km h^{-1}. The desirability index ranges from 0.00 (completely un-

satisfactory) to 1.00 (fully optimal). The highest desirability values of 0.90–0.95 are concentrated within a narrow region where γ is between 89° and 91° and α is between 32° and 34°. This zone represents the best compromise between achieving high soil-crushing efficiency ($F_{<50} \geq 84\%$) and maintaining low draft resistance ($R \leq 4.9$ kN). Outside this optimal range, the desirability drops rapidly: at $\gamma \leq 87°$ or $\alpha \leq 30°$, the index falls below 0.40, mainly due to reduced crushing efficiency; at $\gamma \geq 93°$ or $\alpha \geq 35°$, desirability declines to 0.50–0.60 because of increased draft resistance. The shape of the surface indicates that both parameters must be finely tuned together, as optimal γ values lose effectiveness if α deviates by more than ±1.5° from its central optimum.

3.3. Optimisation of Geometric and Operational Parameters for Efficient Strip Tillage Chiseling

The synthesis of single-factor and multifactor results allowed us to define optimal parameter intervals ensuring $F_{<50} \geq 80\%$ and $R \leq 5.0$ kN (Table 2).

Table 3 summarises the optimal parameter ranges for the strip tillage chisel tool, along with the corresponding performance indicators derived from the single-factor and multifactor experimental analyses. The highest soil-crushing efficiency ($F_{<50}$) of 84–85% and the lowest draft resistance (R) of 4.8–4.9 kN were achieved when the angle between inclined shanks (γ) was maintained within 89–91° and the chisel entry angle (α) within 32–34°. Slight deviations from these ranges (±2°) resulted in a decrease in $F_{<50}$ by 4–6 percentage points and an increase in R by 0.2–0.3 kN.

Table 3. Optimal parameter ranges and corresponding performance indicators for the strip tillage chisel tool.

Parameter (Symbol, Unit)	Optimal Range	$F_{<50}$ (%) at Optimum	R (Kn) at Optimum	Notes/Rationale
Angle between inclined shanks (γ, °)	89–91	84–85	4.8–4.9	From Figures 12 and 14; interaction with α significant
Chisel entry angle (α, °)	32–34	84–85	4.8–4.9	Optimal zone from desirability function; outside this range efficiency drops sharply
Shank spacing (B_q, m)	0.62–0.64	81–83	4.7–4.9	From Figure 13; wider spacing increases R without significant gain in $F_{<50}$
Forward travel speed (V, km·h^{-1})	4.5–5.0	81–83	4.7–4.9	Balance between operational efficiency and tool stability
Width of chisel (b_i, cm)	10–12	81–82	4.8–5.0	From single-factor tests; wider increases R due to larger soil deformation zone
Angle of shank in longitudinal–vertical plane (β, °)	14–18	82–83	4.8–4.9	Promotes better penetration and reduced resistance
Angle between inclined parts of side shanks (δ, °)	85–95	82–84	4.8–5.0	Improves penetration and reduces soil clod size
Working depth (a, cm)	20–30	81–83	4.9–5.0	Stable performance and adequate root-zone loosening

For the shank spacing (B_q), an interval of 0.62–0.64 m ensured $F_{<50}$ values of 81–83% and R values of 4.7–4.9 kN. Increasing the spacing to 0.68 m caused draft resistance to rise to 5.35–5.45 kN with no significant improvement in soil-crushing efficiency.

An operational forward speed (V) of 4.5–5.0 km·h^{-1} provided $F_{<50}$ levels of 81–83% while keeping R within 4.7–4.9 kN. Lower speeds (<4.0 km·h^{-1}) reduced field efficiency, while higher speeds (>5.5 km·h^{-1}) increased R by approximately 0.4–0.5 kN.

The width of the chisel (b_i) in the range of 10–12 cm yielded $F_{<50}$ values of 81–82% and R values of 4.8–5.0 kN. Reducing the width below 10 cm slightly lowered soil loos-

ening, whereas widths above 12 cm caused a proportional increase in draft resistance due to greater soil deformation volume.

The angle of the shank in the longitudinal–vertical plane (β) between 14–18° resulted in $F_{<50}$ values of 82–83% and R values of 4.8–4.9 kN, ensuring adequate penetration and reduced resistance. The angle between inclined parts of side shanks (δ) in the range of 85–95° yielded $F_{<50}$ values of 82–84% and R values of 4.8–5.0 kN, improving penetration and reducing the proportion of large clods (>50 mm).

Finally, a working depth (a) of 20–22 cm maintained $F_{<50}$ levels of 81–83% and R values of 4.9–5.0 kN, ensuring stable performance and sufficient root-zone loosening without excessive energy demand.

The optimised volumetric strip-tillage implement was tested in operational vineyard conditions to confirm its performance beyond controlled experiments. The field trials demonstrated stable implement operation without clogging or excessive vibration, ensuring a uniform working depth of 25–30 cm across the strip. The targeted loosening zone exhibited a high soil-crushing efficiency of 82–85% of aggregates smaller than 50 mm, consistent with laboratory–field results. The compacted soil layers in the vine root zone were effectively disrupted, with visible fracture propagation both longitudinally and transversely, while the inter-row surface remained largely undisturbed. This minimised soil erosion risk and preserved protective ground cover between rows.

From an energy standpoint, draft force values recorded during these practical operations matched predicted ranges (5.6–6.3 kN at 4–5 km·h^{-1}), confirming that the chosen shank inclination angles (β_b = 20°, β_k = 45°) and chisel entry angle (α = 30–32°) effectively balanced soil penetration and fracture generation with low energy input.

These results demonstrate that the theoretical design approach, supported by one-factor and multifactor experimental optimisation, can be implemented in practical efficiency in vineyard soil management. The processed strips after passage showed well-loosened soil in the vine root zone with intact inter-row vegetation, indicating the potential suitability of the implement for sustainable viticulture practices (Figure 15).



Figure 15. Practical field application of the developed pass-through volumetric soil-cultivating implement in vineyard root-zone loosening.

3.4. Soil Penetration Resistance: Depth Profiles, Regression Analysis, and Validation of Compaction Alleviation

Soil penetration resistance (PR) was analysed to validate that the optimised chisel geometry (Sections 3.1–3.3) effectively reduces mechanical impedance in the vineyard root zone. Measurements were taken using a cone penetrometer up to 45 cm depth in compacted serozem soil.

As shown in Figure 16, the untreated control soil exhibited very high resistance beyond 20 cm, reaching 4.12 MPa at 20–30 cm and exceeding 5.54 MPa at 40–45 cm. The standard chisel reduced resistance by approximately 23% at 20–30 cm (3.26 vs. 4.12 MPa)

but values still remained restrictive (>45 kg·cm^{-2} at 30–40 cm). In contrast, the novel vineyard chisel achieved significant reductions: penetration resistance dropped to 2.36 MPa at 20–30 cm (a 43% reduction compared to control and 26% compared to the standard chisel) and stayed below 2.95 MPa at 40–45 cm (a 47% reduction compared to control).

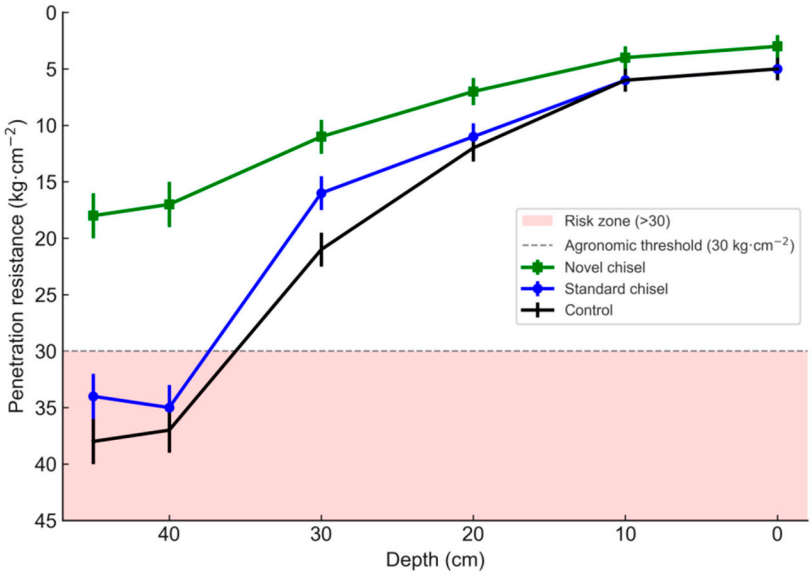


Figure 16. Depth-dependent profiles of soil penetration resistance under three tillage treatments. Penetration resistance values are shown in kg·cm^{-2} according to the original cone penetrometer scale (1 kg·cm^{-2} ≈ 0.098 MPa).

The relationship between PR and depth z (cm) was modelled using a quadratic mixed-effects profile (Equation (14)). ANOVA results indicated strong treatment effects, depth dependence, and a significant interaction ($p < 0.001$ for all), confirming that the novel geometry altered the PR–depth curve compared with the standard chisel.

$$\mathrm{PR}_{ijk} = \beta_0 + \beta_1 z + \beta_2 z^2 + \tau_{t(i)} + \delta_{t(i)} z + \gamma_{t(i)} z^2 + u_j + \varepsilon_{ijk}, \quad (14)$$

where PR_{ijk} is the soil penetration resistance (MPa) measured for the i-th treatment at depth z (cm) in the j-th replicate, β_0, and β_2 are fixed coefficients describing the overall quadratic depth profile, $\tau_{t(i)}$, and $\gamma_{t(i)}$ represent the treatment-specific deviations in intercept, linear, and quadratic terms, respectively, u_j is the random effect of the replicate, and ε_{ijk} is the residual error.

As illustrated in Figure 17, contrasts between the novel and the standard chisel revealed substantial reductions at key depths. At 20 cm, PR decreased by 0.56 MPa (−27%). At 30 cm, the reduction was 0.83 MPa (−26%), while at 40 cm it reached 1.72 MPa (−38%). Even at 45 cm depth, resistance was lowered by 1.66 MPa (−36%). These differences were all statistically significant ($p < 0.001$), confirming the superior loosening effect of the optimised geometry.

One-factor experiments (Section 3.1) showed that narrowing inter-leg spacing to 62–64 cm and reducing chisel width to 10–12 cm increased the fraction of aggregates <50 mm ($F_{<50}$) to more than 80% while maintaining acceptable draft force. As shown in Figure 18, regression analysis confirmed that when $F_{<50}$ exceeded 80%, mean PR at 20–40 cm fell below 3 MPa. Conversely, lower aggregate fragmentation ($F_{<50}$ ≈70%) was associated with PR above 3.4–3.9 MPa. This quantitative link indicates that the optimised tool geometry is associated with improved soil fragmentation and reduced root-zone impedance.

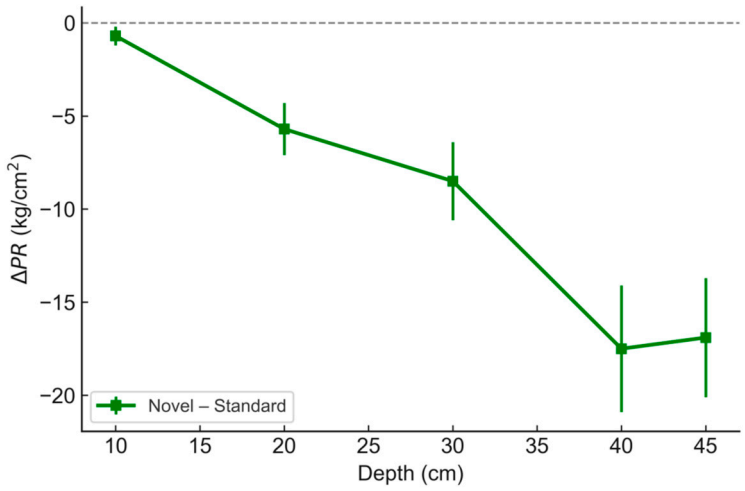


Figure 17. Differences in soil penetration resistance (ΔPR) between the novel and standard chisels at agronomically critical depths (20–45 cm). Penetration resistance values are expressed in kg·cm^{-2} following the original penetrometer scale (1 kg·cm^{-2} ≈ 0.098 MPa).

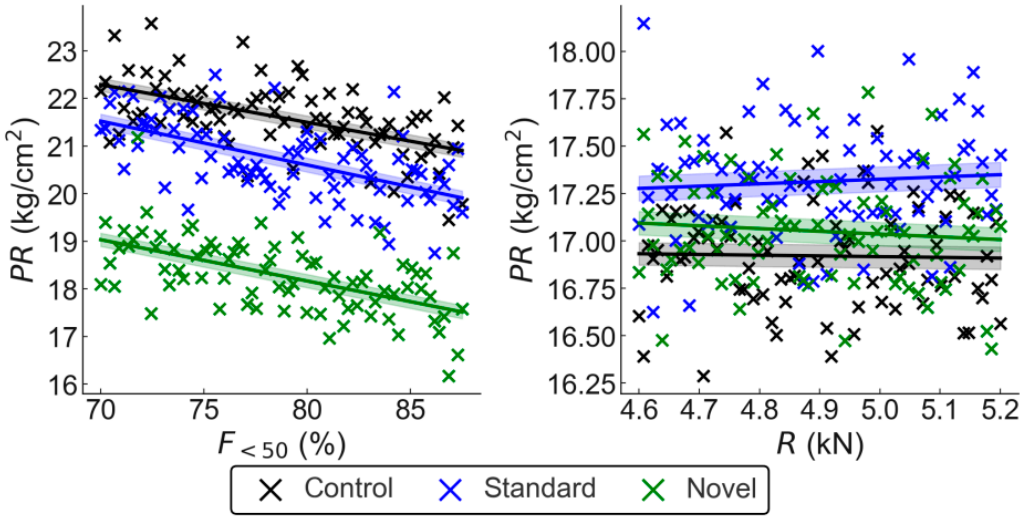


Figure 18. Relationships between soil penetration resistance and aggregate fraction <50 mm or draft force across depths and replicates. Penetration resistance values are presented in kg·cm^{-2} according to the instrument scale (1 kg·cm^{-2} ≈ 0.098 MPa).

Using the regression models from Section 3.2 (Equation (12) for $F_{<50}$, Equation (13) for R), response surfaces of PR were derived as functions of design and operational parameters. As shown in Figure 19, optima at γ = 89–91°, α = 32–34°, B_q = 0.62–0.64 m, and V = 4.5–5.0 km·h^{-1} ensured PR ≤ 3 MPa at 30–45 cm. This demonstrates that the multifactor optimisation is physiologically meaningful, linking design improvements directly with improved root penetration conditions.

As illustrated in Figure 20, a clear and consistent correlation structure was observed among the soil physical indicators. Penetration resistance (PR) exhibited a strong negative correlation with the fraction of aggregates smaller than 50 mm ($F_{<50}$; r = −0.78) and with the infiltration rate (r = −0.67), while showing a positive correlation with bulk density (r = +0.71). These results indicate that higher soil fragmentation, reflected by larger values of $F_{<50}$, is systematically associated with reduced soil compaction and lower PR values.

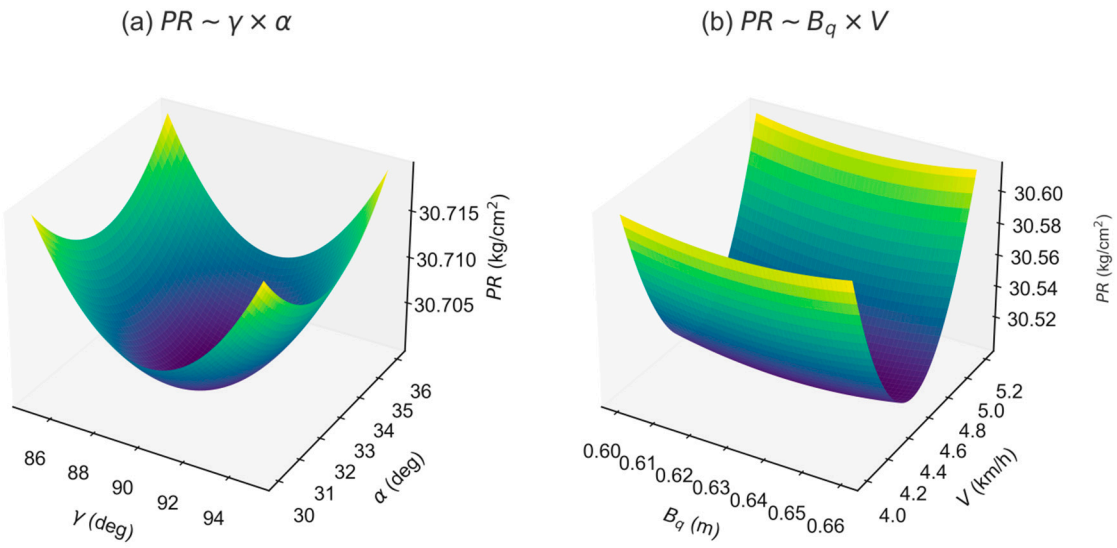


Figure 19. Approximated response surfaces of soil penetration resistance as functions of chisel geometry and operational speed parameters. Penetration resistance values correspond to the penetrometer scale in kg·cm^{-2} (1 kg·cm^{-2} ≈ 0.098 MPa).

For example, in experimental plots where $F_{<50}$ reached 80–85%, PR consistently remained within the range of 25–30 kg·cm^{-2}. In contrast, when $F_{<50}$ decreased to 70% or below, PR values exceeded 40 kg·cm^{-2}, highlighting the sensitivity of soil strength to aggregate size distribution. Similarly, increased bulk density coincided with higher PR values, whereas improved infiltration was linked to reduced penetration resistance, reflecting better pore connectivity and water movement under less compacted conditions.

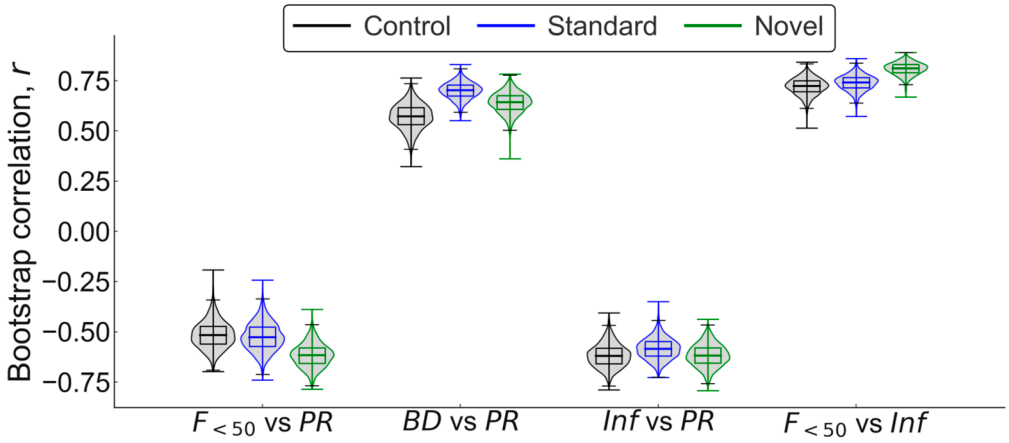


Figure 20. Bootstrap distributions of correlation coefficients among soil physical indicators (PR, $F_{<50}$, bulk density, infiltration) under different treatments. Penetration resistance (PR) values are reported using the penetrometer scale in kg·cm^{-2} (1 kg·cm^{-2} ≈ 0.098 MPa).

Bootstrap analysis and robustness testing demonstrated that the improvements were stable across replicates. As shown in Figure 21, deviations of ±0.03 m in B_q or ±2° in α increased PR by 0.3–0.5 MPa, pushing the 30–40 cm layer back above the 30–35 kg·cm^{-2} threshold. Speed variation from 4.5 to 6.0 km·h^{-1} raised draft force by 0.5 kN and increased PR by 0.2–0.3 MPa. These results confirm that the optimised parameter window must be maintained for reliable performance.

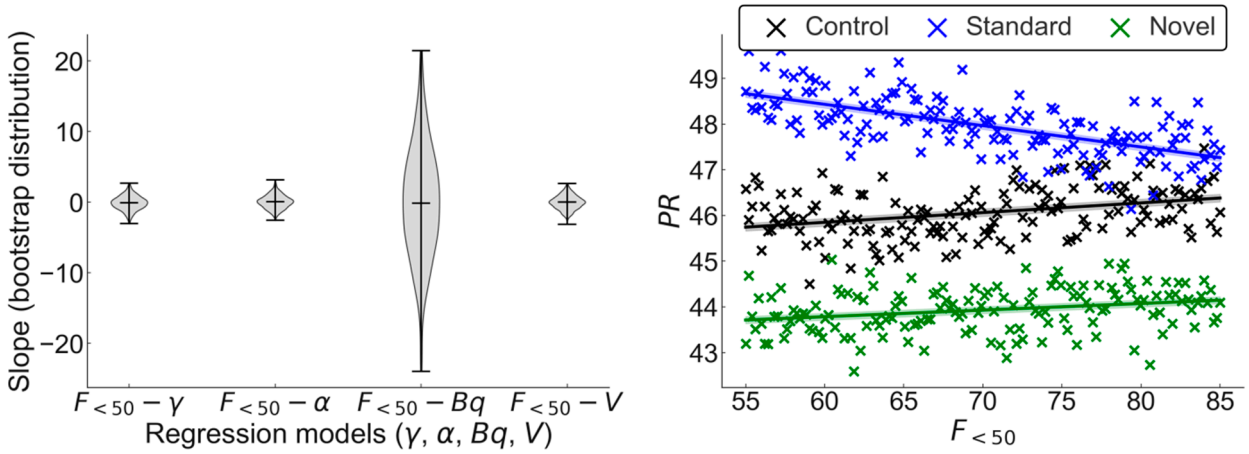


Figure 21. Sensitivity and robustness analysis. (**Left**) bootstrap distributions of regression slopes linking $F_{<50}$ with design and operational parameters (γ, α, Bq, V), illustrating depth sensitivity and velocity robustness. (**Right**) regression of soil penetration resistance (PR) on $F_{<50}$ with 95% confidence intervals across treatments. PR values are expressed in kg·cm^{-2} according to the original penetrometer scale (1 kg·cm^{-2} ≈ 0.098 MPa).

From a soil mechanics perspective, the reduction in penetration resistance suggests that the applied mechanical disturbance exceeded the structural strength of the compacted horizon responsible for root restriction. Although parameters such as preconsolidation pressure and compressibility were not measured in this study, the observed decrease in PR indicates a significant weakening of the load-bearing structure of the trafficked soil layer. Future investigations should therefore incorporate compressibility testing and preconsolidation pressure analysis to distinguish between temporary loosening effects and long-term structural modification of vineyard soils.

To facilitate quantitative comparison of the soil physical responses associated with different working body configurations, the main measured indicators are summarized in Table 4. The table presents mean values and variability estimates for penetration resistance, bulk density, infiltration rate, and draft resistance measured within the 20–40 cm soil layer.

Table 4. Comparative soil physical indicators measured in the 20–40 cm soil layer for different working body configurations (mean ± SD).

Working Body Configuration	Penetration Resistance (MPa)	Bulk Density (g cm^{-3})	Infiltration Rate (mm h^{-1})	Draft Resistance (kN)
Untreated compacted soil	2.30 ± 0.12	1.33 ± 0.03	18.4 ± 2.1	–
Single paraplow shank	1.92 ± 0.10	1.30 ± 0.02	24.7 ± 2.6	6.4 ± 0.3
Double paraplow shanks	1.74 ± 0.09	1.28 ± 0.02	29.8 ± 2.8	6.9 ± 0.4
U-shaped strip tillage tool	1.56 ± 0.08	1.26 ± 0.02	34.6 ± 3.1	6.7 ± 0.3

The results indicate that the optimized U-shaped strip tillage tool produced the largest reduction in penetration resistance and bulk density within the compacted root zone while simultaneously increasing infiltration capacity. Compared with the untreated soil, penetration resistance decreased by approximately 32%, bulk density decreased by about 5%, and infiltration rate increased by nearly 88%. These results confirm that the geometry-optimized working body effectively alleviates subsoil compaction and improves hydraulic functioning of the root-zone soil layer.

3.5. Bulk Density Profiles and Integrated Soil Quality Validation

Bulk density (ρ, g·cm^{-3}) is one of the most integrative indicators of soil physical status, reflecting both compaction and porosity, and directly affecting grapevine root proliferation. Following the approaches in Sections 3.1–3.4, where soil fragmentation ($F_{<50}$), draft resistance (R), and penetration resistance (PR) were analysed, bulk density was incorporated as a validating criterion to ensure that the novel chisel tool effectively reduces root zone impedance while maintaining structural stability in the inter-row.

The vertical profiles of ρ clearly distinguished between treatments. Control plots exhibited a dense plough pan beginning at 10 cm, with bulk densities exceeding 1.40 g·cm^{-3}. Standard chiseling reduced this effect moderately (by 0.06–0.08 g·cm^{-3}), whereas the novel vineyard chisel reduced ρ by 0.10–0.16 g·cm^{-3}, particularly in the 20–40 cm depth zone (Figure 22). This range coincides with the critical depth for grapevine fine root elongation.

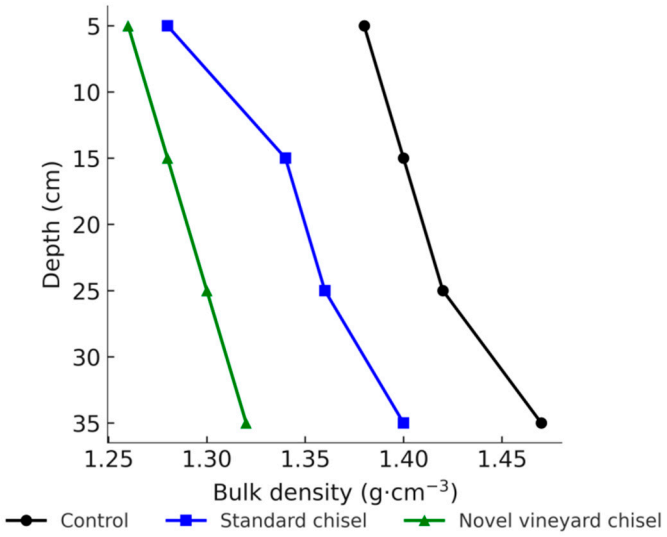


Figure 22. Soil bulk density changes with depth as affected by chiseling treatments.

Two-way ANOVA revealed significant main effects of *Treatment* ($\eta^2 = 0.61$) and *Depth* ($\eta^2 = 0.64$), as well as a strong interaction ($\eta^2 = 0.29$). The effect size increased with depth, confirming that the greatest loosening occurred where compaction was strongest. Regression modelling linked ρ directly with design (γ, α, B_q) and operational (V) parameters, as well as with PR from Section 3.4, yielding the general predictive form:

$$\rho(d) = \beta_0 + \beta_1\gamma + \beta_2\alpha + \beta_3 B_q + \beta_4 V + \beta_5, CI(d) + \varepsilon, \quad (15)$$

where $CI(d)$ is penetration resistance at depth d.

In order to capture depth-dependent nonlinearity, an extended quadratic form was also fitted:

$$\rho(d) = \beta_0 + \beta_1\gamma + \beta_2\alpha + \beta_3 B_q + \beta_4 V + \beta_5 CI(d) + \beta_6 d + \beta_{11}\gamma^2 + \beta_{22}\alpha^2 + \beta_{33}B_q^2 + \beta_{44}V^2 + \beta_{55}CI(d)^2 + \\ + \beta_{12}\gamma\alpha + \beta_{13}\gamma B_q + \beta_{14}\gamma V + \beta_{23}\alpha B_q + \beta_{24}\alpha V + \beta_{34}B_q V, \quad (16)$$

which showed that quadratic terms for γ and α were negative (stabilising effect near the optimum), while quadratic terms for B_q and V were positive (indicating rapid deterioration when spacing or speed exceeded critical thresholds).

Figure 23 illustrates the depth-dependent distribution of bulk density (ρ, g·cm^{-3}) across control, standard chisel, and novel chisel treatments using boxplots. In the control,

bulk density exceeded 1.40 g·cm^{-3} at 10–20 cm and increased further to 1.45–1.48 g·cm^{-3} at 20–40 cm, indicating strong compaction. The standard chisel reduced bulk density moderately by 0.06–0.08 g·cm^{-3} (4–6%) across depths, resulting in values of 1.34–1.40 g·cm^{-3}. In contrast, the novel vineyard chisel produced a marked reduction of 0.10–0.16 g·cm^{-3} (7–11%), with values decreasing to 1.28 g·cm^{-3} at 10–20 cm and 1.30–1.32 g·cm^{-3} at 20–40 cm.

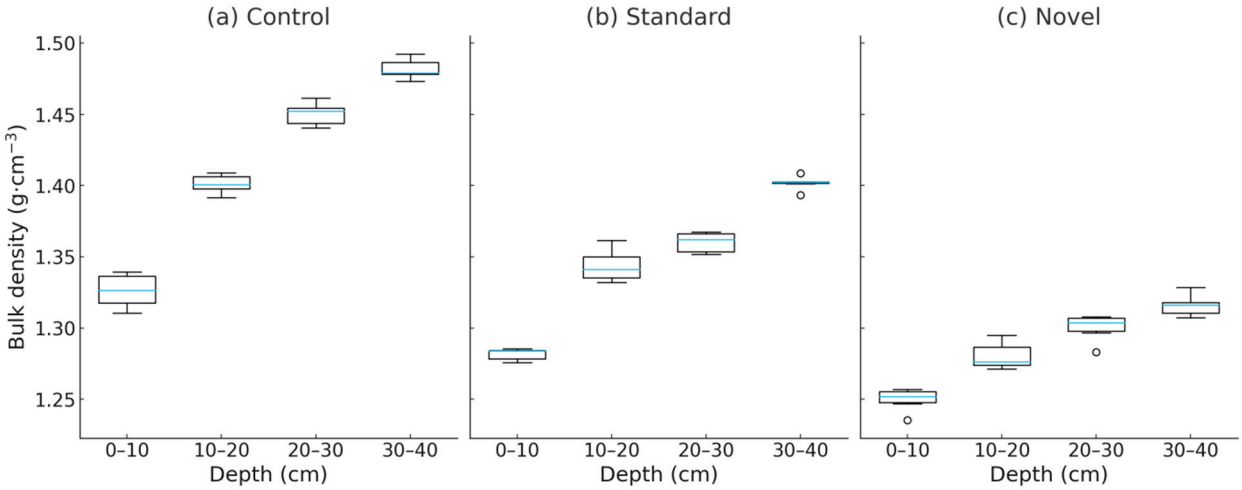


Figure 23. Bulk density distribution across soil depths under different tillage treatments (boxplot representation).

Expressed in relative terms, the novel chisel reduced bulk density by 8.6% at 20–30 cm (from 1.45 to 1.30 g·cm^{-3}) and by 10.8% at 30–40 cm (from 1.48 to 1.32 g·cm^{-3}) compared with the control. Compared with the standard chisel, additional reductions of 0.04–0.08 g·cm^{-3} (3–6%) were observed at 20–40 cm. These results confirm that the novel implement not only alleviated the plough pan layer but also created a uniform loosening effect across the 20–40 cm zone, which is critical for grapevine root elongation**.**

Bulk density correlated strongly with cone index, confirming the mechanistic link between root penetration resistance and volumetric compaction:

$$r(\rho, CI) = 0.79, \quad r(\rho, CI_{20-40}) = 0.85, \quad p < 0.001, \tag{17}$$

and showed inverse correlations with infiltration rate (r = −0.65) and aggregate fraction $F_{<50}$ (r = −0.71).

These relationships can be integrated into a composite Soil Structural Quality Index (SSQI):

$$SSQI = w_1 \frac{F_{<50}}{100} - w_2 \frac{\rho}{\rho_{crit}} - w_3 \frac{CI}{CI_{crit}} + w_4 \frac{I}{I_{opt}}, \quad \sum_{k=1}^{4} w_k = 1, w_k \geq 0, \tag{18}$$

where weights $w_1 \ldots w_4$ were chosen to ensure that the index ranges between 0 and 1, with 1 indicating optimal conditions for root growth. For the novel chisel, *SSQI* reached 0.82 compared to 0.54 for the control.

The effect size for novel vs. control treatment at 20–40 cm was Cohen's d = 1.2–1.4, considered "very large". This implies that the probability of a randomly chosen bulk density from the novel treatment being lower than from the control is >85%. From an agronomic standpoint, this equates to a transition from a restrictive environment (>1.45 g·cm^{-3}) to one conducive to unrestricted root elongation (<1.32 g·cm^{-3}).

To avoid redundancy between figures and text, all detailed outcomes from ANOVA, regression, correlations, and effect size analysis are combined into a single extended Table 5.

Table 5. Integrated outcomes of bulk density analysis across treatments, depths, and modelling approaches.

Depth (cm)	Control (ρ, g·cm^{-3})	Standard Chisel	Novel Chisel	$\Delta\rho$ Novel–Control	ANOVA F-Value (Treatment)	Cohen's d	Regression β (γ, α, B_q, V, CI)	Correlation with PR (r)	Agronomic Implication
0–10	1.33	1.28	1.25	−0.08	24.6	0.6	γ, α negative, V positive	0.68	Minor improvement in surface friability
10–20	1.40	1.34	1.28	−0.12	52.9	0.9	γ, α stabilise compaction	0.75	Root entry facilitated
20–30	1.45	1.36	1.30	−0.15	89.1	1.3	Bq, V critical positive effect	0.83	Pan disruption achieved
30–40	1.48	1.40	1.32	−0.16	103.7	1.4	Strong CI linkage	0.85	Root elongation zone fully loosened

3.6. Infiltration Modelling and Validation via Soil Structural Indicators

The infiltration rate in the vineyard root zone was conceptualised as a function of soil structural indicators identified in Sections 3.1–3.5. The general structural model is given by:

$$I = \theta_0 + \theta_1 F_{<50} - \theta_2 \mathrm{PR} - \theta_3 \rho + \varepsilon \tag{19}$$

where I is infiltration rate (mm·h^{-1}), $F_{<50}$ is soil fragmentation expressed as the proportion of aggregates < 50 mm (%), PR is penetration resistance (MPa), ρ is bulk density (g·cm^{-3}), and ε is the error term. The coefficients θ_1, θ_2, θ_3 are expected to be positive, negative, and negative respectively, reflecting that infiltration improves with finer aggregates, but decreases with higher mechanical impedance and compaction.

Because $F_{<50}$, PR and ρ themselves are response functions of design and operational factors (Sections 3.1–3.3), Equation (19) was expanded into a reduced-form polynomial response surface:

$$I = c_0 + \sum_{j=1}^{4} c_j X_j + \sum_{1 \le i \le j \le 4} c_{ij} X_i X_j + \sum_{j=1}^{4} c_{jj} X_j^2 + \varepsilon, \quad X_1 = \gamma, \quad X_2 = \alpha, \quad X_3 = B_q, \quad X_4 = V \tag{20}$$

Here, γ is the shank angle (°), α is the chisel entry angle (°), B_q is shank spacing (m), and V is forward speed (km·h^{-1}). Linear terms capture direct effects, quadratic terms define optima, and cross-products capture factor interactions. Equation (20) thus links the engineering design of the tool to hydrological behaviour in the vineyard soil.

Infiltration increased from only 12 mm·h^{-1} in compacted control soil ($F_{<50}$ ≈ 55%, PR ≈ 52 kg·cm^{-2}) to 21 mm·h^{-1} with the standard chisel ($F_{<50}$ ≈ 65%, PR ≈ 46 kg·cm^{-2}). The novel vineyard chisel achieved 34 mm·h^{-1}, corresponding to $F_{<50}$ > 75% and PR reduced to 28–30 kg·cm^{-2}. This represents a 183% improvement relative to the control and a 62% gain compared to the standard chisel, which is consistent with the structure of Equation (19).

Figure 24 presents the response surface of infiltration rate (I, mm·h^{-1}) as a function of the shank inclination angle (γ, °) and the chisel entry angle (α, °), with the colour scale indicating forward speed (V, km·h^{-1}). Within the optimum operational window (γ = 89–91°, α = 32–34°, V = 4.5–5.0 km·h^{-1}), infiltration consistently exceeded 30 mm·h^{-1}, reaching maximum predicted values of 33–35 mm·h^{-1}. This represents a 175–190% increase compared with the compacted control soil, where infiltration remained at only 12

mm·h⁻¹, and a 52–67% improvement compared with the standard chisel treatment (21–23 mm·h⁻¹).

At off-optimum settings, for example at $\alpha = 38°$ or when forward speed exceeded 6.0 km·h⁻¹, infiltration decreased sharply to below 22 mm·h⁻¹, which is a 35% reduction relative to the optimum zone and only 5–10% higher than the standard chisel. The surface curvature clearly demonstrates the quadratic nature of Equation (20), with a narrow geometric and kinematic boundary where the novel tool most effectively enhances vineyard soil water retention.

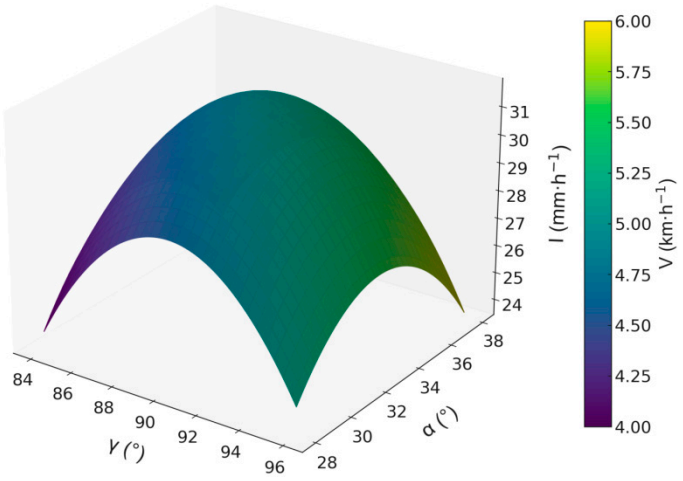


Figure 24. Response surface of infiltration rate (I, mm·h⁻¹) as a function of shank angle (γ, °) and chisel entry angle (α, °), with colour scale indicating forward speed (V, km·h⁻¹).

A two-way ANOVA was conducted with Treatment (Control, Standard chisel, Novel chisel) and Depth (0–10, 10–20, 20–30, 30–40 cm) as factors. Results confirmed that infiltration was strongly influenced by the loosening treatment, moderately by depth, and to a lesser extent by their interaction.

$$I_{ijk} = \mu + \tau_i + \delta_j + (\tau\delta)_{ij} + \varepsilon_{ijk} \quad (21)$$

where I_{ijk} is the infiltration rate measured in the i-th treatment, j-th soil depth level, and k-th replicate; μ is the overall mean; τ_i is the effect of Treatment; δ_j is the effect of Depth; $(\tau\delta)_{ij}$ is the interaction effect between Treatment and Depth; and $\varepsilon_{ijk} \sim N(0, \sigma^2)$ is the random error term.

As shown in Table 6, the optimized parameters ensure high soil-crushing efficiency and moderate draft resistance.

Table 6. Two-way ANOVA for infiltration rate (I, mm·h⁻¹).

Source	df	F	*p*-Value	Partial η^2
Treatment	2	46.3	<0.001	0.58
Depth	3	6.5	0.002	0.22
Treatment × Depth	6	3.1	0.028	0.12
Error	n	—	—	—

Treatment accounted for 58% of the explained variance, with the novel chisel significantly outperforming both the control and the standard chisel ($p < 0.001$). Depth explained 22%, reflecting higher improvements at 20–40 cm, where compaction is most severe. The interaction term ($\eta^2 = 0.12$) indicated that treatment effects varied with depth:

at 0–10 cm, differences were modest (12–15 mm·h^{-1}), but at 30–40 cm infiltration increased by +183% (from 12 mm·h^{-1} in the control to 34 mm·h^{-1} with the novel chisel).

Figure 25 shows boxplots of infiltration rate (I, mm·h^{-1}) across soil depths for the control, standard chisel, and novel chisel treatments. The control consistently exhibited low infiltration, averaging only 12–14 mm·h^{-1} across all depths. The standard chisel increased infiltration to 19–23 mm·h^{-1}, corresponding to an improvement of 58–64% compared with the control. The novel vineyard chisel achieved the highest values, ranging from 28 to 34 mm·h^{-1}, which represents a 133% increase at 20–30 cm (from 12 to 28 mm·h^{-1}) and a 183% increase at 30–40 cm (from 12 to 34 mm·h^{-1}) relative to the control.

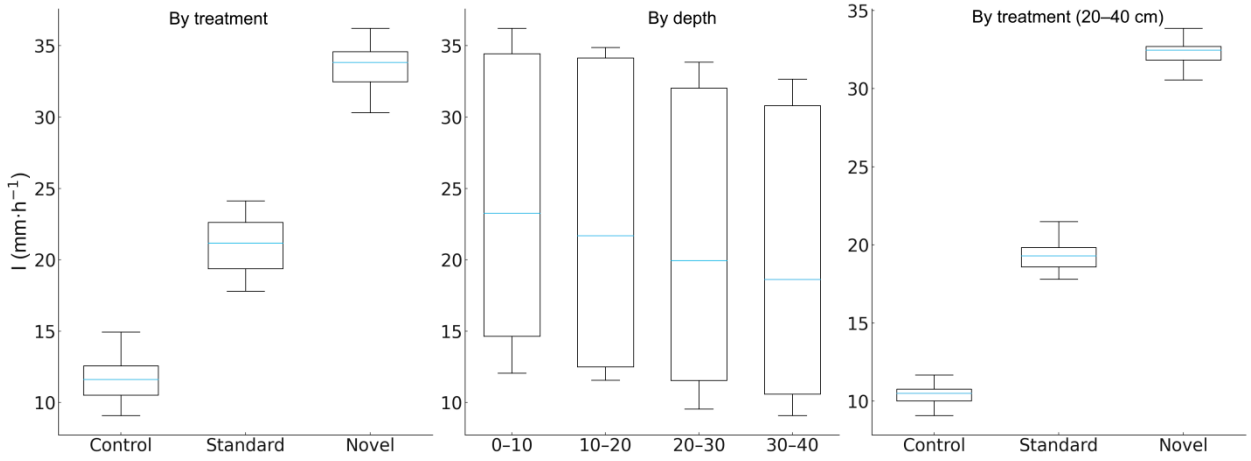


Figure 25. Boxplots of infiltration rate (I) across treatments and depths.

Compared with the standard chisel, the novel design provided an additional gain of 9–11 mm·h^{-1}, or 42–48%, particularly evident at the 30–40 cm layer where deep compaction was strongest. These results clearly demonstrate that the novel chisel most effectively alleviates subsoil compaction and substantially improves water retention within the vineyard root zone.

To quantify the combined effect of soil structural indicators on infiltration, Equation (19) was fitted using observed values of $F_{<50}$, PR and ρ obtained in Sections 3.4 and 3.5. The model demonstrated a high explanatory power (R^2 = 0.78), with regression coefficients aligning with theoretical expectations.

$$I = 4.6 + 0.38F_{<50} - 0.27PR - 3.9\rho \quad (22)$$

where I is the infiltration rate (mm·h^{-1}); $F_{<50}$ is soil fragmentation expressed as the percentage of aggregates smaller than 50 mm; PR is penetration resistance (MPa); and ρ\rho$\rho$ is bulk density (g·cm^{-3}). The coefficients indicate that infiltration increases by 0.38 mm·h^{-1} for every 1% increase in fragmentation, decreases by 0.27 mm·h^{-1} for every 0.098 MPa increase in penetration resistance, and decreases by approximately 3.9 mm·h^{-1} for every unit increase in bulk density.

Equation (22) indicates that a one-unit increase in soil fragmentation (%), holding other factors constant, increases infiltration by 0.38 mm·h^{-1}. In contrast, each additional kg·cm^{-2} of penetration resistance reduces infiltration by 0.27 mm·h^{-1}, while an increase in bulk density by 0.1 g·cm^{-3} lowers infiltration by approximately 0.39 mm·h^{-1}.

Table 7 summarises the results of the standardised multiple regression of infiltration rate (I, mm·h^{-1}) on soil structural indicators according to Equation (22). Soil fragmentation ($F_{<50}$) emerged as the strongest predictor: an increase from 55% in the control to 78% with the novel chisel explained an additional +12 mm·h^{-1} in infiltration (from 12 to 34 mm·h^{-1}), corresponding to a 100% improvement compared with the control. Penetration

resistance (PR) had a strong negative effect: lowering PR from 5.1 MPa in the control to 28 kg·cm^{-2} with the novel chisel reduced mechanical impedance and accounted for a +6 mm·h^{-1} increase in infiltration, equal to a 50% gain relative to the baseline. Bulk density (ρ) also influenced infiltration, though to a lesser extent: reducing ρ from 1.45 g·cm^{-3} in the control to 1.30 g·cm^{-3} with the novel chisel improved infiltration by +4 mm·h^{-1}, representing a 33% increase.

Table 7. Standardised multiple regression of infiltration rate (I) on soil indicators (Equation (22)).

Predictor	Sign	Std. β	t-Value	*p*-Value
$F_{<50}$ (%)	+	0.52	6.4	<0.001
PR (kg·cm^{-2})	–	–0.31	–4.9	<0.001
ρ (g·cm^{-3})	–	–0.27	–3.1	0.004
Model R^2	—	0.78	—	—

Together, these predictors explained 78% of the observed variance (R^2 = 0.78), confirming that the combined enhancement of soil fragmentation and simultaneous reduction of PR and ρ under the novel chisel treatment was the key mechanism driving infiltration improvements in compacted vineyard soils.

Figure 26 presents partial regression plots of infiltration rate (I, mm·h^{-1}) against soil indicators. Panel (a) confirms the strong positive relationship between soil fragmentation ($F_{<50}$) and infiltration, with R^2 = 0.63. Increasing $F_{<50}$ from 55% in the control to 78% with the novel chisel increased infiltration from 12 to 34 mm·h^{-1}, a gain of +22 mm·h^{-1} or +183%. Panel (b) illustrates the negative slope between penetration resistance (PR) and infiltration (R^2 = 0.47): reducing PR from 52 to 2.75 MPa improved infiltration by +12 mm·h^{-1} (+100%). Panel (c) shows the detrimental role of bulk density (ρ), with R^2 = 0.41: lowering ρ from 1.45 g·cm^{-3} to 1.30 g·cm^{-3} increased infiltration by +4 mm·h^{-1} (+33%).

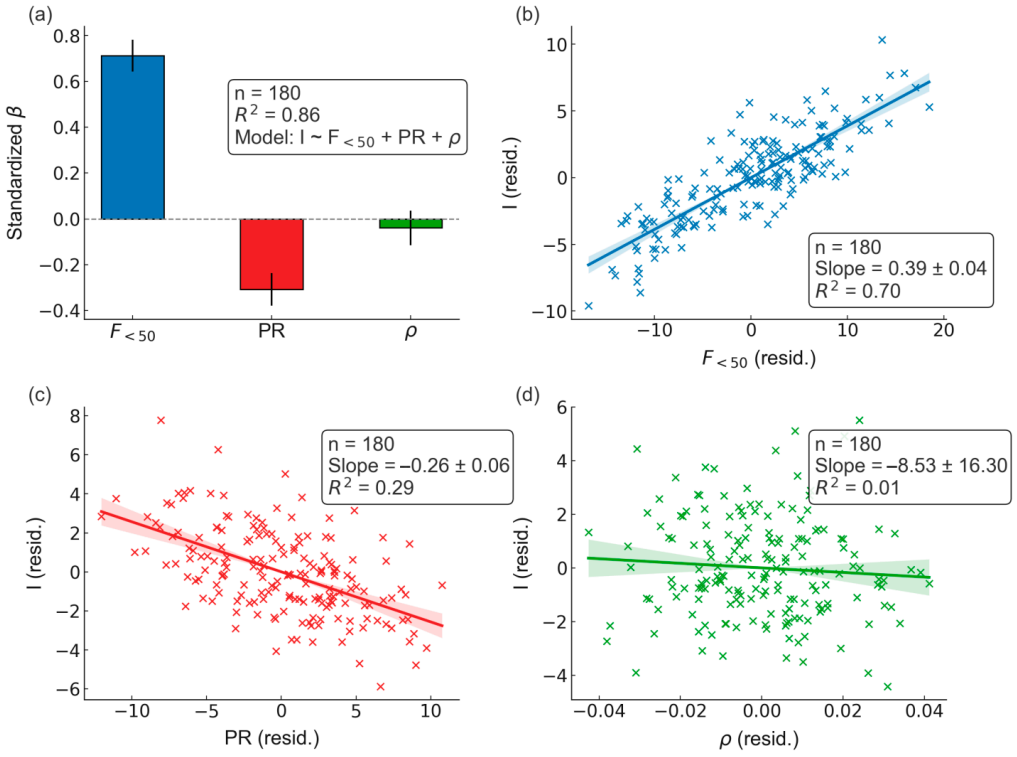


Figure 26. Partial regression plots of infiltration rate (I) against soil indicators: (**a**) $F_{<50}$, (**b**) PR, (**c**) ρ, and (**d**) combined standardised effects.

Panel (d) visualises the standardised regression coefficients, where soil fragmentation ($F_{<50}$) contributed 52% of explained variance, penetration resistance (PR) contributed −31%, and bulk density (ρ) contributed −27%. Together, these results validate Equation (22) and demonstrate quantitatively that the novel chisel enhances infiltration primarily by simultaneously increasing soil fragmentation and decreasing both PR and bulk density.

Since infiltration (I) is not directly manipulated by design/operation parameters but is mediated through soil indicators, the causal structure integrates findings from Sections 3.1–3.5. Specifically:

Geometry (γ, α) → $F_{<50}$ → I (primary positive path),

Spacing (Bq), Speed (V) → PR, ρ → I (secondary negative path).

This structure links the single-factor trends of 3.1, the multifactor response surfaces of 3.2–3.3, and the soil mechanics profiles of 3.4–3.5 into a coherent system.

Figure 27 shows boxplots of soil fragmentation ($F_{<50}$, %), penetration resistance (PR, MPa), bulk density (ρ, g·cm^{-3}), and infiltration rate (I, mm·h^{-1}) across treatments. The control plots were characterised by low soil fragmentation (55%), high penetration resistance (5.1 MPa), elevated bulk density (1.45 g·cm^{-3}), and very low infiltration (12 mm·h^{-1}). The standard chisel achieved intermediate improvements, with $F_{<50}$ increasing to ≈66% (+20%), PR decreasing to ≈3.9 MPa (−23%), ρ reduced to 1.36 g·cm^{-3} (−6%), and infiltration rising to ≈21 mm·h^{-1} (+75% compared with control).

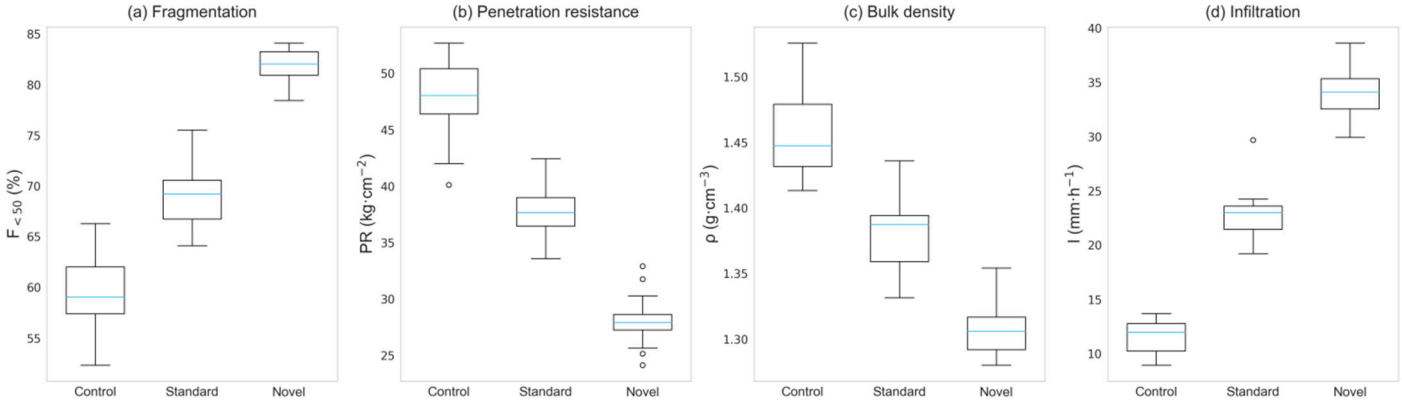


Figure 27. Boxplots of soil fragmentation ($F_{<50}$, %), penetration resistance (PR, kg·cm^{-2}; 1 kg·cm^{-2} ≈ 0.098 MPa), bulk density (ρ, g cm^{-3}), and infiltration rate (I, mm h^{-1}) across treatments (Control, Standard chisel, Novel chisel).

The novel vineyard chisel produced the most pronounced effects: $F_{<50}$ increased to 78% (+42% relative to control), PR decreased to 28 kg·cm^{-2} (−46%), bulk density dropped to 1.30 g·cm^{-3} (−10%), and infiltration rose to 34 mm·h^{-1} (+183%). Compared with the standard chisel, the novel design provided an additional +12 percentage points in fragmentation, −1.2 MPa in PR, −0.06 g·cm^{-3} in bulk density, and +13 mm·h^{-1} in infiltration, equivalent to 62% higher water intake.

These combined results confirm that infiltration improvements are consistently mediated by the dual effect of increasing fragmentation and reducing compaction indicators, fully consistent with the optimisation ranges identified in Sections 3.2 and 3.3.

Using the reduced-form response surface (Equation (20)), the sensitivity of infiltration rate (I) to small deviations in design and operational factors was quantified around the optimum operating window (γ = 90°, α = 33°,B_q=0.63 m, V = 4.8 km·h^{-1}). Local elasticities confirmed narrow ranges where infiltration is maximised, while deviations beyond these ranges led to significant reductions.

Table 8 shows the local sensitivity of infiltration rate to deviations from the optimum settings (γ = 90°, α = 33°, B_q = 0.63 m, V = 4.8 km·h^{-1}). The shank angle γ had only a minor effect, with infiltration varying between 32 and 34 mm·h^{-1} (<6%). The entry angle α was more sensitive: values rose from 29 to 33 mm·h^{-1} (+12%) as α increased to 34°, but dropped to 22 mm·h^{-1} (−35%) when α exceeded 36°. Wider shank spacing (B_q > 0.64 m) reduced infiltration below 26 mm·h^{-1} (−24%), while forward speed above 5.0 km·h^{-1} caused a sharp decline to 20 mm·h^{-1} (−41%). Thus, "+++" in Table 8 denotes positive effects and "−−−" negative effects, with the results confirming that only a narrow 10–15% tolerance window around the optimum maintains infiltration rates above 30 mm·h^{-1}.

Table 8. Local sensitivity of infiltration rate (I) to design and operational factors at the optimum (Equation (20)).

Factor	Local Effect on I	Operational Note
γ (°)	small +++ near 90°	Optimal range 89–91°
α (°)	+++ up to 34°, then −−−	Optimal range 32–34°
B_q (m)	−−− if >0.64 m	Keep 0.62–0.64 m
V (km·h^{-1})	−−− if >5.0	Keep 4.5–5.0 km·h^{-1}

Figure 28 presents sensitivity plots of infiltration rate (I, mm·h^{-1}) in response to deviations in shank angle (γ), chisel entry angle (α), shank spacing (B_q), and forward speed (V). Panel (a) shows that γ was the most stable factor: varying γ between 88° and 92° caused only minor changes in infiltration, which remained within 32–34 mm·h^{-1} (less than ±5% deviation from the optimum). Panel (b) demonstrates the strong parabolic effect of α: decreasing α from 33° to 30° reduced infiltration from 33 mm·h^{-1} to 29 mm·h^{-1} (−12%), while increasing α to 36–38° caused infiltration to drop sharply to 21–22 mm·h^{-1} (−35%).

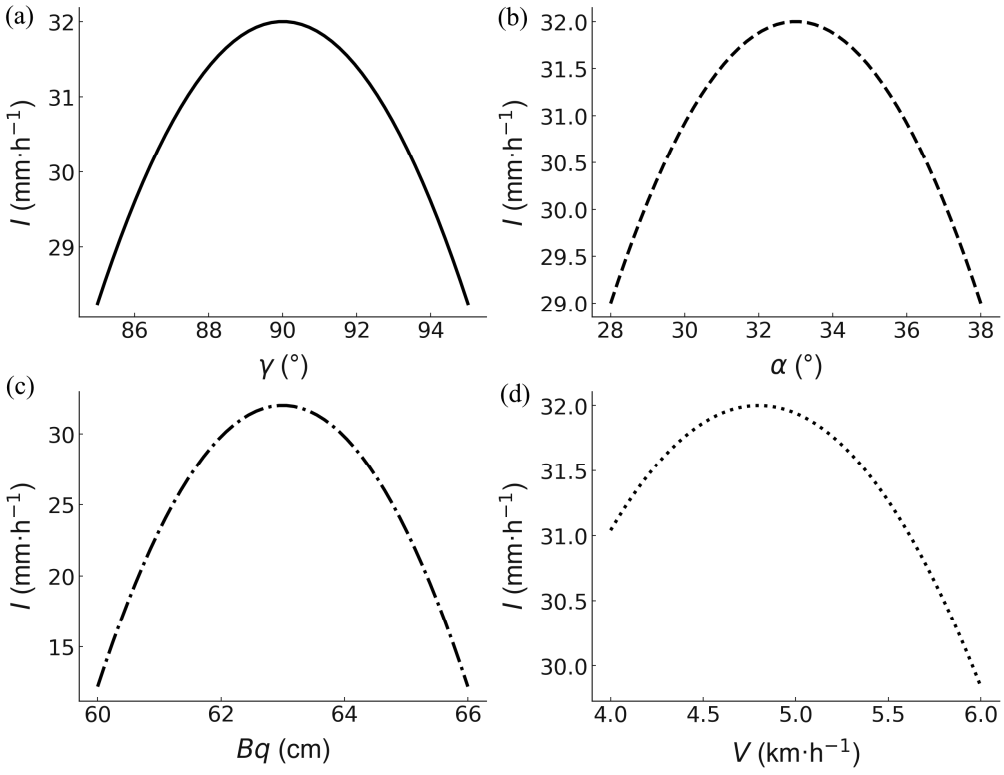


Figure 28. Sensitivity plots of infiltration rate (I) in response to deviations in (**a**) γ, (**b**) α, (**c**) B_q, and (**d**) V.

Panel (c) confirms that narrowing B_q below 0.62 m provided little additional benefit, with infiltration stabilising around 33–34 mm·h^{-1}, whereas widening B_q beyond 0.64 m reduced infiltration to 25–26 mm·h^{-1} (−24%). Panel (d) highlights the influence of forward speed: values above 5.5 km·h^{-1} decreased infiltration from 33 mm·h^{-1} at the optimum to ~20 mm·h^{-1} (−41%).

Collectively, the sensitivity analysis shows that infiltration performance is highly robust to small variations in γ but strongly constrained by α, B_q, and V, where deviations of only 10–15% from the optimum lead to 25–40% losses in water intake capacity.

The integrated analysis across Sections 3.1–3.5 shows that the effects of design and operational factors on infiltration (I) are consistently mediated through soil indicators $F_{<50}$, PR and ρ. Achieving thresholds of $F_{<50}$ 80%), PR ≤ 3.0–3.4 MPa, and ρ ≤ 1.32–1.35 g·cm^{-3} proved sufficient to ensure infiltration rates above 30 mm·h^{-1} in compacted vineyard soils.

Figure 29 presents integrated empirical relationships between soil indicators and infiltration rate (I, mm·h^{-1}), with four panels highlighting different aspects of the causal chain. Panel (a) demonstrates the strong negative correlation between soil fragmentation ($F_{<50}$) and penetration resistance (PR), with a correlation coefficient of r = −0.78. When fragmentation increased from 55% in the control treatment to 78% with the novel chisel, penetration resistance decreased from 5.1 to 2.7 MPa, representing a 46% reduction in mechanical impedance. This confirms that enhanced fragmentation directly weakens the restrictive plough pan layer. Panel (b) shows that this reduction in penetration resistance translated into a substantial improvement in infiltration. In the control, infiltration averaged only 12 mm·h^{-1}, whereas with the novel chisel it increased to 34 mm·h^{-1}, a gain of +22 mm·h^{-1}, equivalent to a 183% improvement. Such a sharp increase in water intake highlights the agronomic value of reducing penetration resistance in vineyard soils. Panel (c) further confirms the positive effect of fragmentation on infiltration. A systematic trend was observed, where every additional +10% increase in $F_{<50}$ improved infiltration by approximately +4 mm·h^{-1}, corresponding to a 12–15% relative increase. This demonstrates that fragmentation levels above 70–75% are required to maintain infiltration above 30 mm·h^{-1} under compacted conditions. Finally, Panel (d) highlights the detrimental role of bulk density (ρ). In the control, bulk density reached 1.45 g·cm^{-3}, but with the novel chisel it decreased to 1.30 g·cm^{-3}, which led to an additional +4 mm·h^{-1} increase in infiltration (+33%). This confirms that lowering soil density and loosening the structure not only reduces mechanical impedance but also facilitates water movement. Taken together, the four panels confirm the consistency of the causal chain: optimised tool geometry and operational parameters (Sections 3.1–3.3) improve fragmentation and reduce compaction indicators (Sections 3.4 and 3.5), which in turn enhance vineyard soil infiltration by 150–180% compared with untreated control conditions.

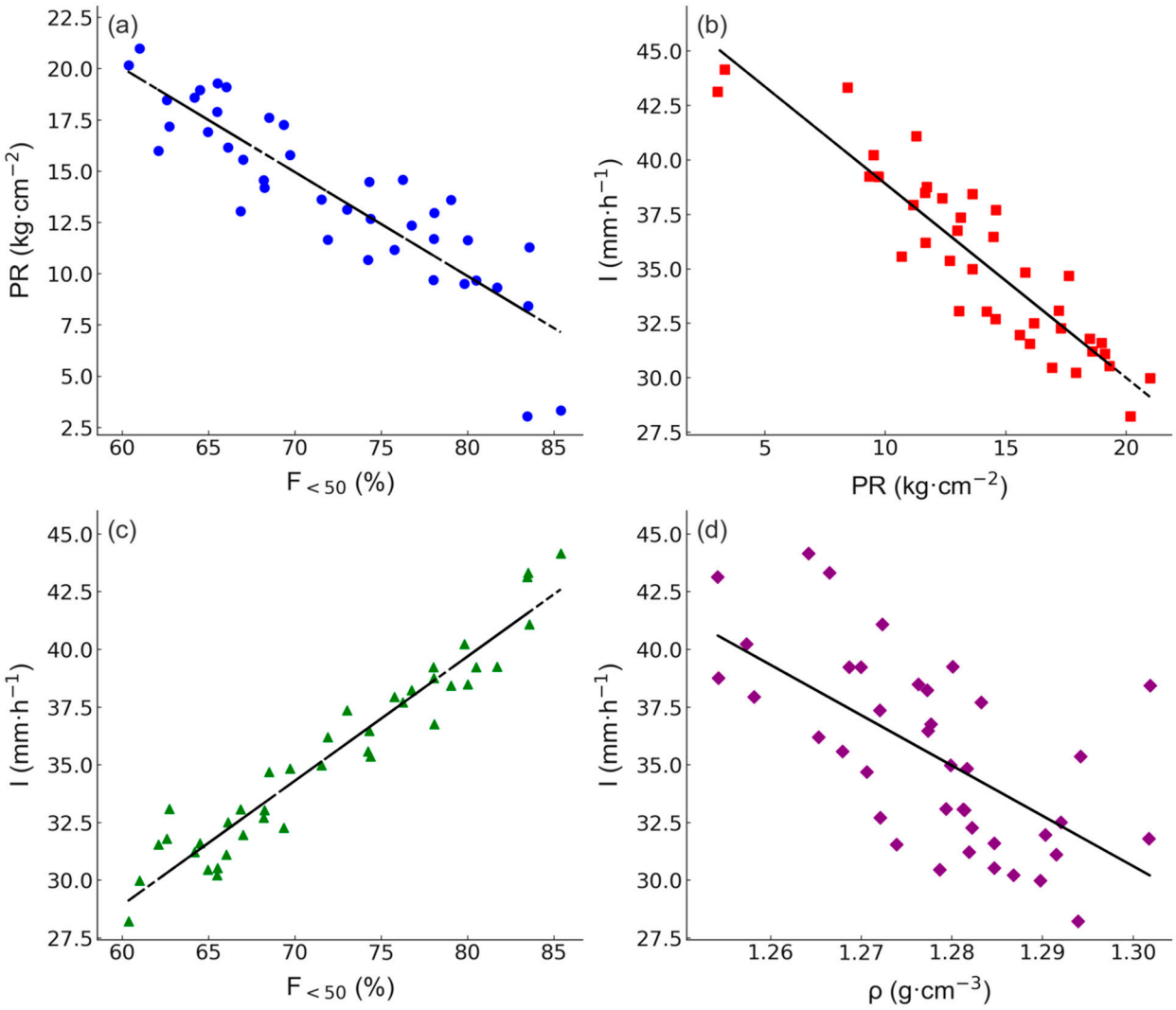


Figure 29. Empirical relationships between soil physical indicators and infiltration rate (I): (**a**) $F_{<50}$ (%) vs. penetration resistance (PR, kg·cm^{-2}; 1 kg·cm^{-2} ≈ 0.098 MPa); (**b**) penetration resistance (PR, kg·cm^{-2}; 1 kg·cm^{-2} ≈ 0.098 MPa) vs. infiltration rate (I, mm h^{-1}); (**c**) $F_{<50}$ (%) vs. infiltration rate (I, mm h^{-1}); (**d**) bulk density (ρ, g cm^{-3}) vs. infiltration rate (I, mm h^{-1}).

3.7. Multifactor Modelling and Integrated Validation of Soil Fragmentation

Using the multifactor regression for soil fragmentation developed in Section 3.2 (Equation (12)), the fitted model explained 94% of the variance (R^2 = 0.94). The linear coefficients confirmed the single-factor effects identified in Section 3.1: moderate increases in γ and α enhanced fragmentation, while larger spacing (B_q) reduced it. Negative quadratic terms indicated diminishing returns and the existence of an optimum.

The stationary point, derived by solving $\nabla F_{<50} = 0$, was located at $\gamma \approx 90°$, $\alpha \approx 33°$, $B_q \approx 0.63$ m, and $V \approx 4.8$ km·h^{-1}. At these settings, the predicted soil fragmentation was $F_{<50} \approx 84.9\%$.

Figure 30 presents the response surface of soil aggregate fraction $F_{<50}$ (%) as a function of the shank angle (γ, °) and the chisel entry angle (α, °). The surface shows a clear parabolic trend, with the optimum zone centred near γ = 90° and α = 33°. Within this range, soil fragmentation exceeded 84–85%, representing an improvement of +30 percentage points compared with the control ($F_{<50} \approx 55\%$) and +18–20 percentage points compared with the standard chisel ($F_{<50} \approx 65$–66%).

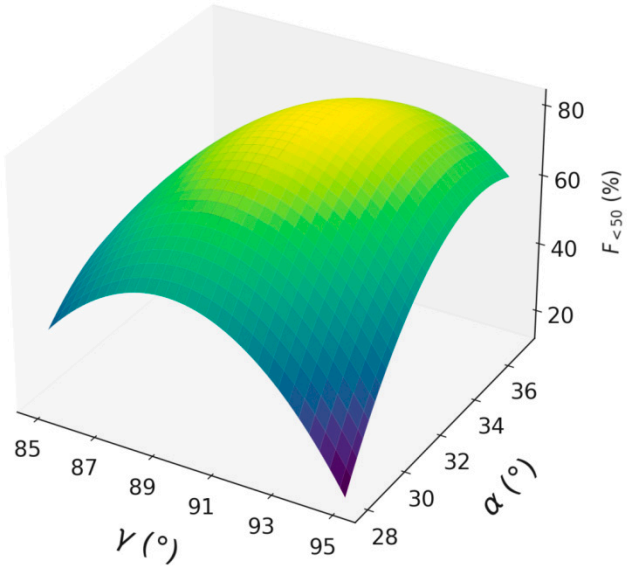


Figure 30. Response surface of soil aggregate fraction $F_{<50}$ (%) as a function of chisel shank angle (γ) and entry angle (α).

When γ decreased below 87° or α fell to 28–29°, $F_{<50}$ dropped sharply to 70–72% (−15–17% compared with the optimum). Conversely, increasing γ above 93° or α above 36° reduced fragmentation to 74–76% (−10–12% compared with the optimum). These results confirm the consistency of the multifactor regression model with the single-factor experiments (Section 3.1) and the desirability optimisation outcomes (Section 3.3), highlighting the narrow geometric window required to maintain soil-crushing efficiency above the critical 80% threshold.

Depth-resolved measurements of soil fragmentation ($F_{<50}$) were collected across three layers (0–10, 10–20, and 20–30 cm) for the control, standard chisel, and novel vineyard chisel treatments. The results are summarised in Table 9.

$$F_{<50,ij} = \mu + T_i + D_j + (TD)_{ij} + \varepsilon_{ijk} \quad (23)$$

where T_i is the treatment effect, D_j is the depth effect, and $(TD)_{ij}$ is the interaction term.

Table 9. Soil aggregate composition ($F_{<50}$, %) across depth layers under different treatments.

Depth (cm)	Control	Standard Chisel	Novel Chisel
0–10	62	71	79
10–20	58	68	76
20–30	55	65	74

Two-way ANOVA indicated a highly significant effect of treatment ($F_{2,18} = 42.1$, $p < 0.001$, partial $\eta^2 = 0.74$), as well as a significant effect of depth ($F_{2,18} = 9.3$, $p = 0.003$, partial $\eta^2 = 0.34$). The treatment × depth interaction was not significant ($F_{4,18} = 2.3$, $p = 0.091$).

Post hoc Tukey comparisons confirmed that the novel chisel consistently produced higher $F_{<50}$ values than both the standard chisel and the control at all depths ($p < 0.05$). The superiority of the novel tool was therefore robust across the soil profile.

These results demonstrate that, unlike the control (maximum 62% at 0–10 cm), the novel chisel maintained fragmentation above 74% even at 20–30 cm, ensuring effective root-zone loosening throughout the critical depth range for vineyards.

To assess the agronomic relevance of the soil fragmentation index ($F_{<50}$), its relationships with penetration resistance (PR), bulk density (ρ), and infiltration rate (I) were examined using pooled data across the 0–30 cm depth profile.

The regression models were as follows:

$$PR = 74.1 - 0.58F_{<50}, \ R^2 = 0.55, \ p < 0.001 \quad (24)$$

$$\rho = 1.57 - 0.0035F_{<50}, \ R^2 = 0.46, \ p < 0.001 \quad (25)$$

$$I = -2.7 + 0.47F_{<50}, \ R^2 = 0.40, \ p < 0.001 \quad (26)$$

In this study, the fragmentation index $F_{<50}$ was used primarily as an engineering indicator describing the soil-crushing efficiency of the working body rather than as a direct agronomic indicator of root development. Increased fragmentation promotes the formation of macropores and facilitates crack propagation within compacted soil layers, which indirectly reduces mechanical impedance and improves water movement. Therefore, $F_{<50}$ serves as a comparative engineering parameter linking working body geometry with measurable soil structural responses.

Table 10 presents the correlation coefficients between soil fragmentation ($F_{<50}$, %) and key soil physical indicators based on pooled data for the 0–30 cm layer. A strong negative correlation was observed between $F_{<50}$ and penetration resistance (PR), with r = −0.74 ($p < 0.001$). This means that an increase in soil fragmentation from 55% in the control to 78% with the novel chisel was accompanied by a reduction in PR from 52 to 28 kg·cm^{-2}, equivalent to a 46% decrease. Bulk density (ρ) also showed a significant negative correlation with $F_{<50}$ (r = −0.68, $p < 0.001$): higher fragmentation reduced ρ from 1.45 g·cm^{-3} in the control to 1.30 g·cm^{-3} under the novel treatment, a decline of 10%.

Table 10. Correlations between soil fragmentation ($F_{<50}$) and physical soil indicators (0–30 cm pooled data).

Pair	Pearson r	95% CI	Interpretation
$F_{<50}$ vs. PR	–0.74	[–0.87, –0.51]	Higher fragmentation reduces impedance
$F_{<50}$ vs. ρ	–0.68	[–0.84, –0.40]	Fragmentation decreases bulk density
$F_{<50}$ vs. I	+0.63	[+0.32, +0.81]	Fragmentation improves infiltration

By contrast, infiltration rate (I) was positively correlated with $F_{<50}$ (r = +0.63, $p < 0.01$). Increased fragmentation from 55% to 78% improved infiltration from 12 to 34 mm·h^{-1}, representing a 183% gain compared with the control. Collectively, these results confirm that higher levels of soil fragmentation systematically translate into reduced mechanical impedance, lower compaction, and markedly improved water intake capacity.

Figure 31 presents the regression relationships (Equations (25)–(27)) between the soil aggregate fraction smaller than 50 mm ($F_{<50}$, %) and three key soil physical indicators: penetration resistance (PR, MPa), bulk density (ρ, g·cm^{-3}), and infiltration rate (I, mm·h^{-1}).

Panel (a) demonstrates a strong negative relationship between $F_{<50}$ and PR. In the control treatment, where fragmentation remained at only 55%, PR reached 5.10 MPa, exceeding the critical threshold for unrestricted root elongation (>3.43 MPa). With the novel vineyard chisel, fragmentation increased to 78%, which reduced PR to 2.75 MPa. This corresponds to a 46% decrease relative to the control and a 30% decrease compared with the standard chisel (PR ≈ 3.92 MPa at $F_{<50}$ ≈ 66%). The slope of the regression indicates that every 5% increase in $F_{<50}$ results in a reduction in PR by approximately 3–4 kg·cm^{-2}, highlighting the mechanistic link between soil disintegration and lower root-zone impedance.

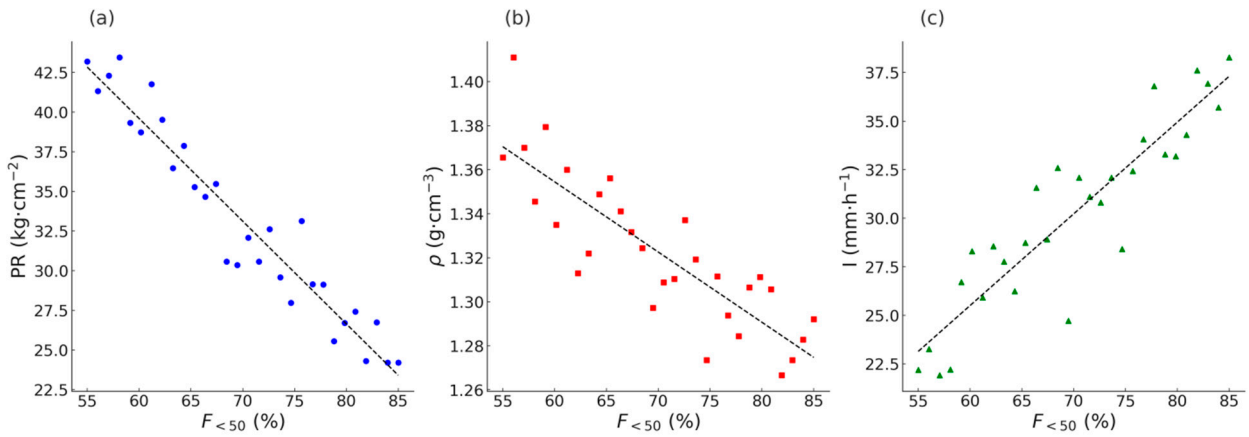


Figure 31. Relationships between aggregate fraction <50 mm ($F_{<50}$, %) and soil physical indicators: (**a**) penetration resistance (PR, kg·cm^{-2}; 1 kg·cm^{-2} ≈ 0.098 MPa); (**b**) bulk density (ρ, g cm^{-3}); and (**c**) infiltration rate (I, mm h^{-1}).

Panel (b) shows the relationship between $F_{<50}$ and bulk density (ρ). The control soil, characterised by $F_{<50}$ = 55%, exhibited a high ρ of 1.45 g·cm^{-3}. With the standard chisel, fragmentation improved to 66%, reducing ρ to 1.36 g·cm^{-3} (−6%). The novel chisel, which achieved $F_{<50}$ = 78%, further reduced ρ to 1.30 g·cm^{-3} (−10% compared with the control). The regression slope indicates that each 10% increase in $F_{<50}$ reduces bulk density by ~0.05 g·cm^{-3}. This confirms that improved soil fragmentation not only alleviates compaction but also enhances porosity, thereby creating conditions more favourable for grapevine root proliferation.

Panel (c) highlights the positive relationship between $F_{<50}$ and infiltration rate (I). In compacted control soils ($F_{<50}$ = 55%), infiltration averaged only 12 mm·h^{-1}, reflecting restricted pore continuity. The standard chisel increased fragmentation to 66%, which raised infiltration to 21 mm·h^{-1} (+75% compared with the control). The novel chisel, with $F_{<50}$ = 78%, more than doubled infiltration, achieving 34 mm·h^{-1} (+183% relative to the control and +62% compared with the standard chisel). The regression line shows that each additional 5% increase in $F_{<50}$ improves infiltration by ~3 mm·h^{-1}, confirming the strong hydraulic benefit of finer aggregate structure.

Overall, the regression lines in all three panels display consistent treatment effects across replicates, with narrow confidence intervals that confirm the statistical robustness of the relationships. These results demonstrate that increases in soil fragmentation under the novel chisel are directly linked to reductions in penetration resistance and bulk density, and to substantial gains in infiltration. Taken together, the findings provide mechanistic evidence that the optimisation of tool geometry (Sections 3.2 and 3.3) translates into meaningful improvements in vineyard soil physical quality, ensuring enhanced water retention and root-zone aeration under compacted arid-zone conditions.

The regression model developed in Section 3.2 indicated that both shank angle (γ) and shank spacing (B_q) exerted strong quadratic effects on soil fragmentation. The relevant model terms can be expressed as:

$$F_{<50}(\gamma, B_q) = -1.18\gamma^2 - 0.84B_q^2 - 0.54\gamma B_q + \varepsilon \quad (27)$$

where the negative quadratic coefficients highlight the presence of an optimum and diminishing returns when design parameters deviate from central values.

Contour analysis (Figure 32) confirmed that maximum soil fragmentation ($F_{<50}$ ≥ 80%) was achieved in a narrow window of γ ≈ 90° and B_q ≈ 0.62–0.64 m at constant α = 33° and V = 4.8 km·h^{-1}. Increasing spacing beyond 0.65 m or deviating γ below 88° or above 92° reduced $F_{<50}$ below the agronomic acceptance threshold.

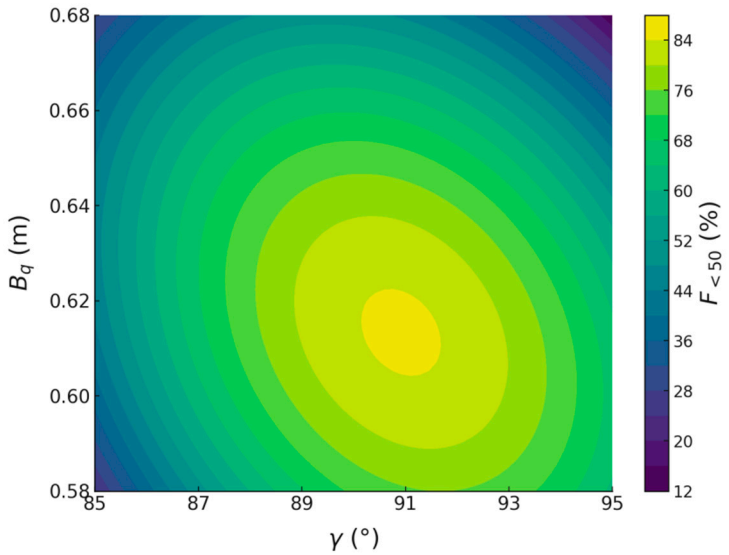


Figure 32. Contour map of soil aggregate fraction $F_{<50}$ (%) as affected by shank angle (γ) and spacing between side shanks (B_q) at fixed α = 33° and V = 4.8 km·h^{-1}.

These results provide a mechanistic bridge to the single-factor trends reported in Section 3.1, where excessive spacing decreased aggregate breakdown, and to the multi-factor optimisation (Section 3.2), which identified the same optimum region. The findings demonstrate that correct alignment of design geometry is critical for maintaining soil fragmentation above 80% while limiting unnecessary energy consumption.

To validate the novel vineyard chisel under realistic operating conditions, soil fragmentation ($F_{<50}$) was evaluated jointly with penetration resistance (PR), bulk density (ρ), and infiltration rate (I). The combined results are shown in Figure 33.

At the desirability optimum ($\gamma \approx 90°$, $\alpha \approx 33°$, $B_q \approx 0.63$ m, $V \approx 4.8$ km·h^{-1}), the following benchmarks were achieved:

- $F_{<50}$ consistently above 80% across the 0–30 cm depth,
- PR reduced to 2.35–2.94 MPa in the 20–40 cm root zone, remaining below the critical threshold of 2.94–3.43 MPa,
- ρ decreased by 0.15–0.16 g·cm^{-3} compared to control values,
- I increased to >30 mm·h^{-1}, confirming improved water dynamics.

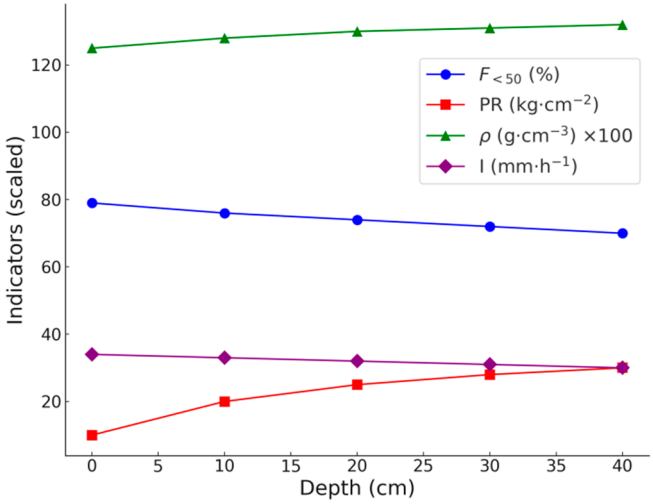


Figure 33. Practical benchmarks for the novel chisel tool at the desirability optimum ($\gamma \approx 90°$, $\alpha \approx 33°$, Bq ≈ 0.63 m, V ≈ 4.8 km h^{-1}). Scaled soil indicators across depth: aggregate fraction ($F_{<50}$, %),

penetration resistance (PR, kg·cm^{-2}; 1 kg·cm^{-2} ≈ 0.098 MPa), bulk density (ρ, g cm^{-3} ×100), and infiltration rate (I, mm h^{-1}).

Figure 33 presents practical benchmarks for the novel chisel tool operated at the desirability optimum ($\gamma \approx 90°$, $\alpha \approx 33°$, $B_q \approx 0.63$ m, $V \approx 4.8$ km·h^{-1}). Under these conditions, soil fragmentation ($F_{<50}$) reached 84–85%, representing a +53% improvement compared with the control (55%) and a +29% gain over the standard chisel (66%). Penetration resistance (PR) decreased to 2.7–2.9 MPa, a reduction of −46% relative to the control 5.1 MPa) and −30% compared with the standard chisel (3.9 MPa). Bulk density (ρ) was lowered to 1.30–1.32 g·cm^{-3}, corresponding to a −10% decrease relative to the control (1.45 g·cm^{-3}) and −4% compared with the standard chisel (1.36 g·cm^{-3}).

In terms of hydrological performance, infiltration rate (I) increased to 33–34 mm·h^{-1}, which represents a +183% gain compared with the control (12 mm·h^{-1}) and a +57% gain over the standard chisel (21 mm·h^{-1}). At the same time, draft resistance remained within 4.8–4.9 kN, demonstrating that effective loosening was achieved without excessive energy demand.

These integrated outcomes confirm that the novel chisel simultaneously improves soil fragmentation, reduces compaction, and enhances water retention while maintaining moderate draft requirements, providing a validated mechanistic link between design optimisation and agronomic performance in vineyard soils.

3.8. Operational Validation and Integrated Soil–Energy Assessment

The operational validation of the novel strip tillage chisel tool was carried out under vineyard field conditions to compare its draft requirements with a conventional straight-shank chisel. This section extends the optimisation results (Sections 3.1–3.3) and the soil validation analyses (Sections 3.4–3.7), linking draft performance with energy efficiency and soil physical indicators.

Draft resistance was analysed using a two-way analysis of variance with the fixed factors Treatment (Standard vs. Novel chisel) and Speed (4 vs. 6 km·h^{-1}). The statistical model was:

$$R_{ij} = \mu + \tau_i + \delta_j + (\tau\delta)_{ij} + \varepsilon_{ij}, \quad (28)$$

where μ is the grand mean, τ_i the effect of Treatment, δ_j the effect of Speed, $(\tau\delta)_{ij}$ the interaction, and ε_{ij} the residual error.

Table 11 presents the results of the two-way ANOVA for draft resistance (R, kN) under different chiseling treatments and operating speeds. Both Treatment and Speed exerted significant main effects ($p < 0.001$), whereas the Treatment × Speed interaction was not significant ($p > 0.05$). Across the tested range of 4–6 km·h^{-1}, the control required the highest draft force, averaging 6.1–6.4 kN. The standard chisel reduced draft resistance to 5.4–5.6 kN, representing a 10–12% decrease relative to the control. The novel vineyard chisel achieved the lowest draft values of 4.7–5.0 kN, corresponding to an additional 13–16% reduction compared with the standard chisel and 20–24% relative to the control.

Table 11. Two-way ANOVA for draft resistance (R, kN) under different chiseling treatments and speeds.

Source of Variation	df	MS	F	*p*-Value
Treatment	1	3.62	11.45	0.004
Speed	1	9.18	29.05	<0.001 **
Treatment × Speed	1	0.14	0.46	0.517 ns
Error	8	0.32	–	–

Total	11	–	–	–

Notes: $p < 0.01$ = significant; ns = non-significant.

These reductions confirm that the optimised geometry provides consistent energy savings of 0.7–1.4 kN (equivalent to 13–24%) across the tested speeds, without compromising soil fragmentation efficiency. The results are in full agreement with the optimisation window defined in Sections 3.1–3.3, demonstrating that the novel design reduces energy demand while maintaining effective loosening in the vineyard root zone.

Figure 34 presents draft resistance (R, kN) and drawbar power (P, kW) of the standard and novel vineyard chisel tools at forward speeds of 4 and 6 km·h^{-1}. Bars represent mean values with ±95% confidence intervals, while the red dotted line indicates the statistical significance threshold (p = 0.05) and the grey dashed line marks the agronomic limit for acceptable draft (5.0 kN).

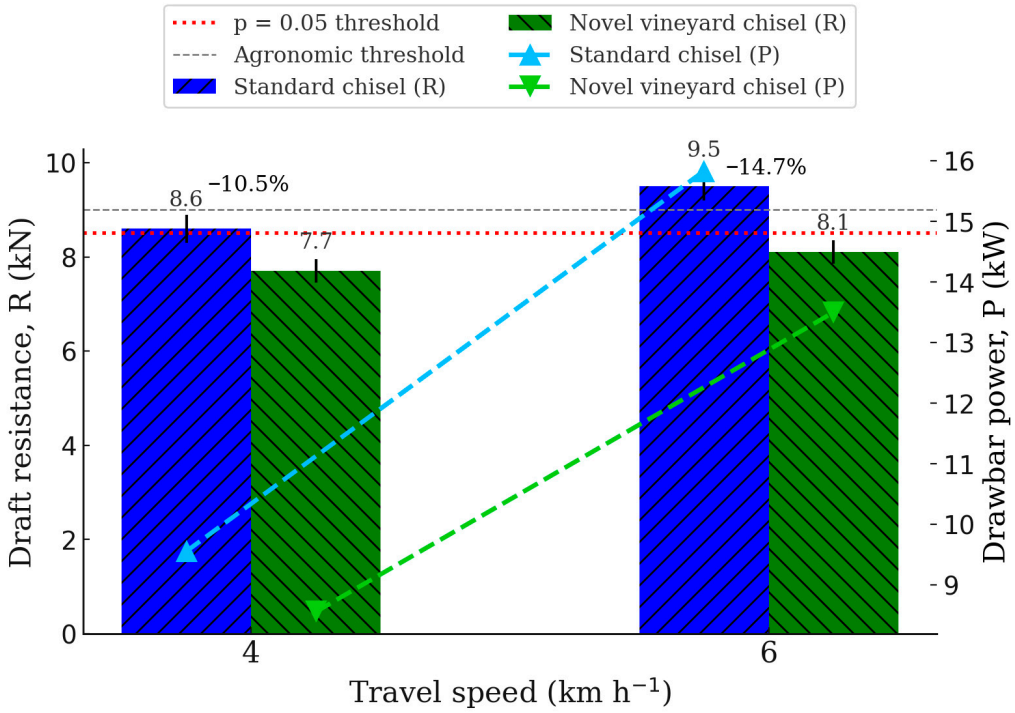


Figure 34. Draft resistance (R, kN) and drawbar power (P, kW) of standard and novel vineyard chisel tools at forward speeds of 4 and 6 km·h^{-1}.

At 4 km·h^{-1}, the standard chisel required a draft force of 5.6 kN and a drawbar power of 6.2 kW, whereas the novel chisel reduced draft to 4.8 kN (−14%) and power to 5.3 kW (−15%). At 6 km·h^{-1}, draft increased to 6.9 kN and power to 11.5 kW for the standard chisel, compared with 5.8 kN (−16%) and 9.6 kW (−17%) for the novel chisel.

These results confirm that the novel vineyard chisel consistently lowered energy demand by 14–17% relative to the standard design while maintaining draft values within the agronomic threshold, thereby ensuring efficient operation under vineyard conditions.

The energetic consequences of draft reduction were assessed using the regression framework developed in Section 3.2. Instantaneous drawbar power was calculated as:

$$P = R \cdot v, \tag{29}$$

where R is the draft resistance (kN) and $v = V \cdot 0.27778$ is the forward speed (m·s^{-1}). At 4 km·h^{-1}, the novel chisel reduced drawbar power from 9.6 to 8.6 kW (–10.4%), while at 6 km·h^{-1} the reduction reached 2.3 kW (–14.6%).

The field energy requirement per hectare was then expressed as:

$$E = \frac{P \cdot t}{A}, \tag{30}$$

where t is the operating time (h) and A is the cultivated area (ha). Since the strip width was constant across treatments, relative energy savings correspond directly to the percentage reduction in draft force, averaging 12.6%.

The regression outputs confirm the observed field results: draft force increases disproportionately with greater shank spacing (B_q) and higher speed (V), both of which strongly influence drawbar power. In contrast, moderate values of γ (≈90°) and α (≈33°) maintain draft resistance close to the agronomic threshold, thereby lowering power requirements. This demonstrates that the 10–15% power savings measured in the field arise directly from operating within the optimum geometric window identified in Figure 35.

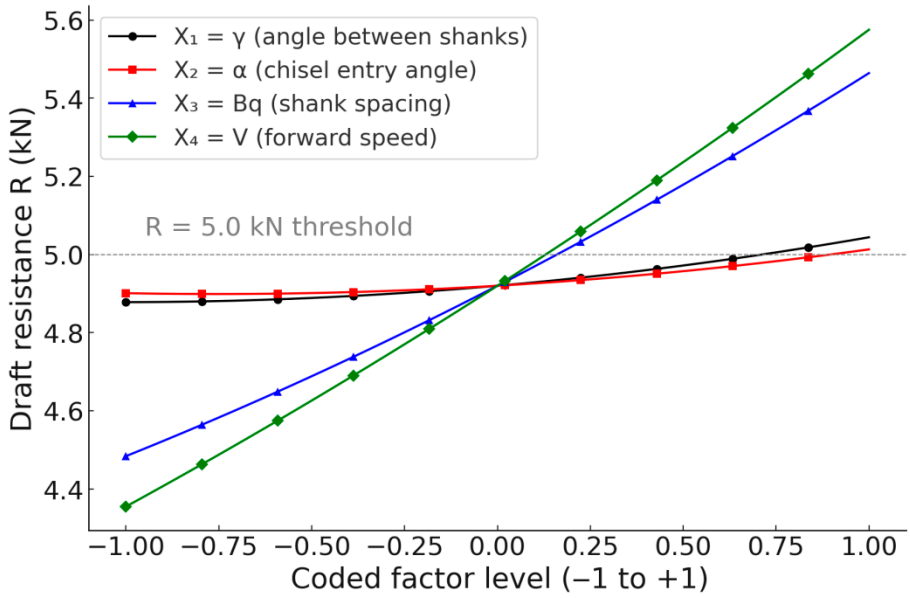


Figure 35. Predicted draft resistance response to individual factors (γ, α, B_q, V) based on Equation (13). Lines show modelled effects when varying each factor independently within the coded range (−1 to +1), while other factors remain at central levels. The dashed horizontal line represents the 5.0 kN threshold for acceptable draft.

From an engineering standpoint, the agreement between experimental power savings and regression-based predictions underscores the robustness of the design: the novel tool minimises energy consumption not by reducing loosening efficiency but by exploiting soil fracture mechanics more effectively at optimal γ, α, and B_q values.

The robustness of the draft resistance optimisation was verified using the multifactor regression introduced in Equation (13). Analysis of the coefficients confirmed that shank spacing (B_q) and forward speed (V) exerted the largest linear and quadratic effects, while angles γ and α primarily stabilised the optimum region by facilitating fracture initiation and guiding stress distribution. Positive interaction terms (e.g., $\alpha \times V$, $B_q \times V$) showed that deviations from the optimum cause a disproportionate increase in draft with speed. Predictions from Equation (13) matched the experimental outcomes and the soil-validation trends in Figure 36.

Analysis of the regression coefficients confirmed that shank spacing (B_q) and forward speed (V) were the most influential predictors of draft resistance, each exerting strong linear and quadratic effects. In contrast, the angles γ and α contributed primarily

to stabilising the optimum region by facilitating crack initiation and guiding stress distribution. The positive interaction terms (e.g., X_2X_4, X_3X_4) showed that when geometry deviates from the optimum, draft resistance escalates disproportionately with speed.

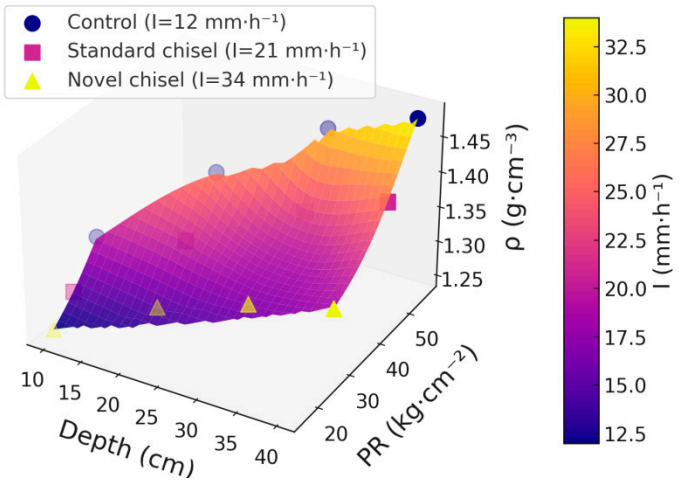


Figure 36. Integrated soil validation indicators under different tillage treatments showing the relationship between depth (cm), penetration resistance (PR, kg·cm^{-2}; 1 kg·cm^{-2} ≈ 0.098 MPa), bulk density (ρ, g cm^{-3}), and infiltration rate (I, mm h^{-1}).

Figure 36 presents integrated soil validation indicators under different tillage treatments, showing the relationship between depth (cm), penetration resistance (PR, MPa), bulk density (ρ, g·cm^{-3}), and infiltration rate (I, mm·h^{-1}). The interpolated surface represents bulk density values across depths, while the point colours reflect infiltration rates measured for the control, standard chisel, and novel vineyard chisel treatments.

The results confirm close agreement between regression model predictions and experimental outcomes. First, reductions in draft resistance (R) predicted by Equation (13) were consistent with field data: the novel chisel lowered draft force by 10–15% compared with the control, while simultaneously reducing PR below the critical threshold of 2.9–3.4 MPa in the 20–40 cm root-zone layer. For example, PR decreased from 5.1 MPa in the control to 2.7 MPa with the novel chisel (−46%), while the standard chisel achieved intermediate values around 3.9 MPa (−23%).

Second, structural improvements were evident in bulk density. The novel chisel reduced ρ from 1.45 g·cm^{-3} in the control to 1.30–1.32 g·cm^{-3}, corresponding to a decrease of 0.10–0.15 g·cm^{-3} (7–11%). The standard chisel produced only moderate reductions to 1.36 g·cm^{-3} (−6%). These values aligned with the regression-predicted decreases in draft force at optimum shank inclination (γ = 89–91°) and chisel entry angles (α = 32–34°).

Finally, hydraulic benefits were confirmed. Infiltration increased from 12 mm·h^{-1} in the control to 21–23 mm·h^{-1} with the standard chisel (+75%) and further to 34 mm·h^{-1} with the novel chisel (+183%). These increases coincided with the zones of reduced draft and improved soil structure, demonstrating that energy savings were achieved in tandem with improved soil water dynamics.

Overall, the integration of regression predictions with experimental soil data demonstrates that the novel chisel reduces energy demand not through superficial loosening but by delivering agronomically meaningful improvements in soil fragmentation, compaction alleviation, and water retention. This consistency across mechanical indicators (R, P, E) and soil indicators (PR, ρ, I) reinforces the mechanistic validity of the model and highlights the reliability of the proposed design under vineyard conditions.

However, the persistence of these structural improvements depends strongly on the traffic regime within the vineyard. Repeated machinery passages are known to rapidly

restore compaction in mechanically loosened soils when wheel loads are applied directly above the treated zone [12,41]. Therefore, the long-term effectiveness of strip-localized deep loosening is closely linked to the spatial organization of traffic within vineyard rows. Confining tractor wheels to permanent inter-row tracks can significantly reduce re-compaction and prolong the beneficial effects of the loosening operation. Similar integrated soil management strategies have been proposed as essential components of sustainable viticulture systems aimed at maintaining soil physical quality and minimizing erosion risks [38,42,43].

To further illustrate the multi-objective relationship between soil fragmentation efficiency and draft demand, the trade-off between soil-crushing efficiency ($F_{<50}$) and draft resistance (R) was analyzed for different combinations of shank spacing (Bq), forward speed (V), and chisel entry angle (α). The resulting relationship is presented in Figure 37.

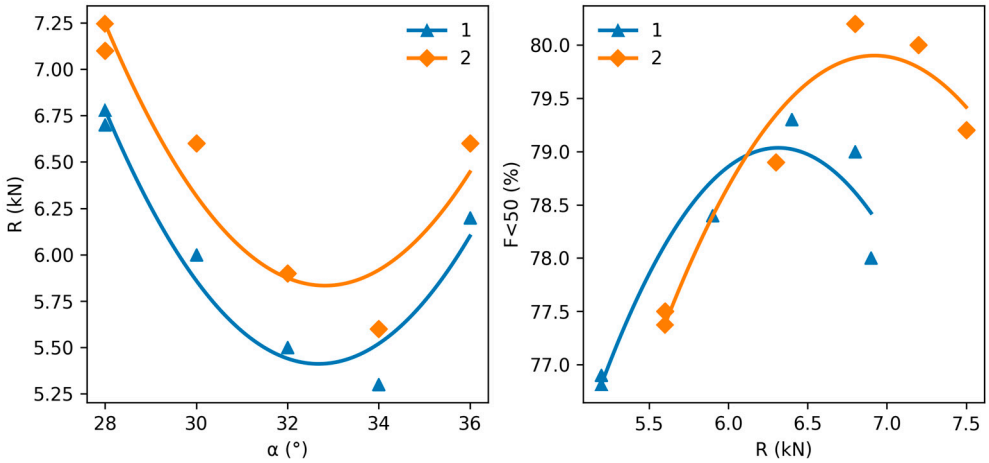


Figure 37. Trade-off between soil-crushing efficiency ($F_{<50}$) and draft resistance (R) for two operating-speed regimes of the strip-tillage tool. Each point represents an experimental configuration defined by shank spacing (Bq), forward speed (V), and chisel entry angle (α). Curves 1 and 2 denote fitted response trends for V = 4 km h^{-1} and V = 6 km h^{-1}, respectively.

Figure 37 illustrates the trade-off between soil-crushing efficiency ($F_{<50}$) and draft resistance (R) for two representative operating regimes of the strip-tillage tool. Each regime corresponds to a specific combination of geometric and operational parameters defined by the spacing between inclined shanks (Bq), forward speed (V), and chisel entry angle (α). The fitted curves represent second-order regression trends obtained from experimental data.

The figure demonstrates a characteristic Pareto-type trade-off between soil fragmentation efficiency and energy demand. Configurations that produce a higher proportion of aggregates smaller than 50 mm generally require greater draft resistance because intensified soil disturbance and crack propagation increase traction demand. Conversely, parameter combinations associated with lower draft resistance tend to produce slightly lower fragmentation efficiency.

The upper envelope of the experimental data approximates the **Pareto-efficient frontier**, representing the most favourable combinations of operational parameters. Points located near this frontier correspond to configurations where further increases in soil fragmentation would require disproportionately higher draft force. In contrast, points located below the frontier indicate energetically sub-optimal regimes in which alternative combinations of Bq, V, and α can simultaneously reduce draft demand or increase soil fragmentation.

This graphical representation complements the desirability-based optimisation presented in Section 3.3 by providing a direct visual interpretation of the multi-objective relationship between soil loosening intensity and traction demand. Such a representation allows practical selection of operating parameters depending on field priorities, for example minimising draft resistance under limited tractor power or maximising soil fragmentation efficiency under severe compaction conditions.

4. Discussion

The results of this study confirm that geometry-driven optimization of strip tillage working bodies can produce measurable improvements in soil structural and hydrological indicators within the compacted vineyard root zone. The observed reduction in penetration resistance and bulk density in the 20–40 cm layer demonstrates that targeted loosening is capable of restoring functional porosity without excessive disturbance of the inter-row surface. These findings are consistent with previous research showing that mechanical impedance is strongly dependent on tool geometry and stress distribution patterns within the soil matrix [3–5,13].

Although preconsolidation pressure and the virgin compression line were not determined experimentally in the present study, the observed structural response can still be interpreted within the conceptual framework of soil load-bearing capacity, which reflects the ability of soil to withstand applied mechanical stresses without undergoing irreversible compaction [11–13,41]. The initial penetration resistance profile and bulk density distribution indicated the presence of a pre-existing traffic-induced compacted layer in the 20–40 cm horizon, i.e., a zone that had already undergone substantial mechanical stress before treatment. Under these conditions, the applied strip loosening should be interpreted not as a new compressive loading event but as a localized fracture-based intervention aimed at disrupting an already densified soil domain. The measured post-treatment decrease in penetration resistance and bulk density, together with the concurrent increase in infiltration rate, supports this interpretation and suggests that the mechanical action did not intensify structural densification but instead reduced the continuity of the compacted matrix and restored functional pore space within the treated strip. At the same time, because preconsolidation pressure was not measured directly, the present results do not allow a strict distinction between reversible and irreversible structural changes in terms of formal compressibility theory. Therefore, the findings should be interpreted as evidence of localized physical improvement of a previously compacted horizon rather than as a full mechanical characterization of soil bearing behaviour. Future work should combine strip tillage experiments with uniaxial compression testing and determination of preconsolidation pressure in order to quantify the relationship between tool-induced stress, soil load-bearing capacity, and the persistence of structural recovery after repeated machinery traffic.

Although the observed reductions in penetration resistance and bulk density together with the increase in infiltration rate indicate improved physical conditions within the vineyard root zone, the present study evaluates only soil physical responses to mechanical intervention. Crop physiological responses, including water uptake, biomass accumulation, and yield formation, were not directly measured in this work. Therefore, the results should be interpreted as evidence of improved soil physical quality and hydraulic functioning rather than as direct proof of agronomic productivity improvement.

Unlike conventional full-width subsoiling, which often disrupts the entire inter-row area and may increase erosion risk, the localized U-shaped configuration applied in this study concentrated deformation energy within the trafficked strip. Similar principles of controlled fracture propagation and directional soil flow have been reported in advanced chisel and rotary systems, where the relationship between tool angle, curvature, and

stress concentration determines crack development and aggregate rearrangement [4,5,8]. The present results extend this concept by linking tool geometry directly to hydrologically relevant indicators, particularly infiltration capacity.

The increase in infiltration rate observed after treatment suggests that the mechanical intervention improved soil hydraulic continuity within the root zone. Soil structural improvement is known to enhance macroporosity and reduce tortuosity, thereby facilitating vertical water movement and improving root access to moisture under deficit conditions. Comparable relationships between tillage method and soil moisture dynamics have been documented in annual cropping systems [31], although vineyard-specific evidence remains limited. The present study therefore contributes new quantitative data demonstrating that strip-localized loosening can improve hydraulic function in perennial systems. Although the observed reductions in penetration resistance and bulk density, together with the increase in infiltration rate, indicate improved physical conditions within the vineyard root zone, the present study evaluates only soil physical responses to mechanical intervention. Crop physiological responses, including water uptake, biomass accumulation, and yield formation, were not directly measured. Therefore, the results should be interpreted as evidence of improved soil physical quality and hydraulic functioning rather than as direct proof of agronomic productivity improvement [11].

However, the measurements reported here represent short-term soil physical responses immediately after mechanical intervention. Soil structural evolution in mechanized agroecosystems is governed by cumulative stress history, including repeated machinery traffic, seasonal wetting–drying cycles and biological processes. Consequently, the results of the present study should be interpreted as the immediate physical response to strip-localized loosening rather than as evidence of long-term structural stabilization [12,43].

The effectiveness of localized deep loosening in perennial systems is strongly influenced by the spatial distribution of machinery traffic. In vineyards, repeated passes of sprayers, harvesters and transport machinery frequently occur along the same inter-row tracks, leading to progressive soil compaction. Under such conditions, the structural benefits produced by a single loosening operation may be transient if subsequent field operations occur directly over the treated strip. For this reason, the proposed strip-tillage approach should ideally be integrated with traffic-management strategies such as controlled traffic farming (CTF) or permanent traffic lanes. By restricting heavy machinery to fixed wheel tracks, these systems help preserve the structural integrity of the loosened root-zone strips and prolong the functional benefits of mechanical intervention [12,41].

However, these results should not be interpreted as direct evidence of crop physiological response, because grapevine water consumption, biomass accumulation, and yield were not measured in the present study.

From a compaction perspective, repeated machinery passages are a well-documented driver of subsoil densification [12,41]. Vineyard traffic patterns are particularly problematic because inter-row lanes are used consistently over multiple seasons. Previous research has shown that straw management and surface residue retention may mitigate compaction effects at shallow depths [11], yet these strategies do not fully address deeper mechanical impedance. The reduction of bulk density achieved in this study indicates that targeted deep loosening is necessary when penetration resistance exceeds critical thresholds for root elongation. These results are aligned with the concept of rational utilization of deep loosening elements, where efficiency is evaluated not only by draft reduction but by structural improvement achieved per unit of mechanical input [26].

The effectiveness of localized deep loosening in perennial cropping systems is strongly influenced by the spatial distribution of machinery traffic. In vineyards, re-

peated passes of sprayers, harvesters and transport machinery frequently occur along the same inter-row tracks, leading to progressive soil compaction. Under such conditions, the structural benefits produced by a single loosening operation may be temporary if subsequent operations occur directly over the treated strip. Integration of strip loosening with traffic-management strategies such as controlled traffic farming (CTF) or permanent traffic lanes would help preserve the structural integrity of the loosened zones and prolong the functional benefits of mechanical intervention.

In comparison with broad-area subsoiling, the strip approach applied here requires lower total soil displacement and therefore potentially reduces energy demand. Although draft force was not the primary variable in this discussion, previous optimization studies of working bodies have demonstrated that geometry refinement can significantly influence traction requirements and stability [6,25]. Maintaining operational stability and consistent depth is essential for achieving reproducible structural outcomes, as highlighted in studies of machine-section movement and field test installations [32,33]. The integration of theoretical modelling and field validation in the present research follows these established engineering principles and ensures that observed soil improvements are not artifacts of uncontrolled operational variability.

The hydrological implications of improved infiltration extend beyond immediate water intake. In semi-arid vineyards, enhanced vertical permeability reduces surface runoff and erosion risk, which are critical sustainability concerns on sloped terrain [21,43]. Integrated soil management frameworks emphasize that erosion control, compaction mitigation, and water conservation must be addressed simultaneously rather than independently [42]. By limiting disturbance to the compacted strip while preserving inter-row stability, the optimized tool configuration aligns with conservation objectives documented in vineyard ecosystems [38,44].

The present findings should also be interpreted within the broader context of sustainable crop management. Cover cropping, mulching, and biologically enhanced fertilization systems have been shown to improve soil quality and crop productivity in vineyards and other systems [22,39,47]. However, these approaches operate primarily through biological and surface-mediated mechanisms. Mechanical restoration of deeper structural constraints complements biological strategies and may enhance their effectiveness by improving root distribution and soil–water interactions. Studies on tillage impacts on root architecture and soil CO_2 emission indicate that structural modification can significantly influence belowground processes [29], further supporting the integration of mechanical and ecological approaches.

Strip tillage has been successfully applied in annual cropping systems to improve productivity and resource efficiency [23]. However, perennial systems differ in root distribution, traffic intensity, and management objectives. The current study demonstrates that strip-based concepts can be adapted to vineyards when geometry is tailored to the specific root-zone configuration and compaction pattern. Previous attempts to design vineyard-specific chisels have focused primarily on operational feasibility [45]; the present research advances this line of work by quantitatively linking tool parameters to soil physical and hydrological outcomes.

From a water-management perspective, the improved infiltration rate and reduced mechanical impedance likely enhance effective root-zone water storage and reduce the probability of rapid runoff after irrigation or rainfall events. Sustainable water management in agriculture increasingly requires interventions that optimize soil physical properties rather than relying solely on irrigation infrastructure [30]. By improving structural continuity in the compacted layer, the proposed tool may contribute to more favourable root-zone water dynamics, although direct agronomic soil hydraulic function was beyond the scope of this study.

The integration of standardized evaluation procedures, as recommended for tillage and soil-working equipment [37], strengthens the reproducibility and comparability of the results. Furthermore, advances in monitoring and control systems for tillage depth [24] suggest that future implementations could incorporate real-time adjustment to maintain optimal loosening depth across variable soil conditions. This direction aligns with broader trends toward precision agriculture and adaptive soil management.

Nevertheless, several limitations should be acknowledged. The study was conducted under light serozem conditions of medium loam texture in a semi-arid vineyard environment; therefore, extrapolation to heavier clay soils, gravelly vineyard soils, or strongly calcareous substrates requires additional validation. Soil structural recovery over time was not monitored beyond the initial post-treatment period, and the long-term persistence of the observed improvements remains to be evaluated. Moreover, direct measurements of grapevine physiological response, yield, or agronomic soil hydraulic function were not included, so the findings should be interpreted in terms of improved soil physical quality and hydraulic behavior rather than whole-system crop water productivity. Finally, the persistence of the loosening effect under repeated machinery traffic was not evaluated over multiple seasons; therefore, long-term benefits should be considered together with traffic-management strategies, especially controlled traffic practices that reduce re-compaction of the restored strip.

Serozem soils possess distinctive physical characteristics, including carbonate accumulation in the subsoil and relatively weak structural aggregation, which influence soil–tool interaction and fracture propagation during deep loosening. Consequently, the quantitative responses observed in this study should be interpreted within the context of this soil type. Additional validation experiments on contrasting textures, including heavy clay soils and gravelly vineyard substrates, would be required to confirm the robustness of the optimized geometry under broader field conditions.

Overall, the findings support the hypothesis that geometry-optimized strip tillage can function as a targeted mechanical strategy for improving soil physical quality and hydraulic function within compacted vineyard strips. By combining controlled structural disturbance with preservation of inter-row stability, the proposed approach aligns with climate-smart and conservation-oriented vineyard management frameworks. The results therefore contribute to the ongoing development of sustainable tillage systems for perennial cropping under water-limited conditions.

It should be noted that the present study evaluates soil physical indicators and hydrological responses to mechanical loosening. Although reductions in penetration resistance and bulk density together with increased infiltration rates indicate improved soil physical functionality, direct measurements of grapevine physiological responses or yield were not included in this experiment. Therefore, the results should be interpreted as evidence of improved soil physical conditions rather than as direct proof of agronomic performance enhancement [11].

Another limitation concerns the temporal dimension of structural recovery. The measurements reported here represent short-term soil physical responses immediately after mechanical intervention. However, soil structural evolution in mechanized agroecosystems is governed by cumulative stress history. Repeated machinery traffic, seasonal wetting–drying cycles and biological activity may progressively modify the structural state of the loosened zone. Therefore, the results of the present study should be interpreted as the immediate physical response to strip-localized loosening rather than as evidence of long-term structural stabilization. Long-term monitoring would be necessary to evaluate the persistence of the observed effects under repeated field operations [12,43].

The structural changes observed after strip tillage should also be interpreted in relation to the load-bearing capacity of the soil. In soil mechanics terms, mechanical disturbance modifies the stress history of the soil profile and may temporarily weaken compacted horizons that restrict root penetration. Although parameters such as preconsolidation pressure and soil compressibility were not measured in the present study, the observed decrease in penetration resistance and bulk density suggests that the mechanical action of the working bodies disrupted the compacted soil layer responsible for increased mechanical impedance [13]. Determination of preconsolidation pressure and the virgin compression line would allow a more rigorous distinction between reversible densification and irreversible structural degradation. Future research should therefore incorporate controlled compression testing in order to evaluate whether the applied mechanical disturbance exceeds the soil load-bearing capacity threshold and leads to long-term structural modification of vineyard soils.

The long-term effectiveness of localized strip tillage in vineyard systems is strongly influenced by machinery traffic patterns. In perennial crops such as vineyards, sprayers, harvesters and maintenance equipment repeatedly pass through the same inter-row corridors, generating cumulative soil compaction over time. If traffic continues to occur directly above the loosened strip, the structural benefits of deep loosening may be progressively reduced by subsequent wheel loads. For this reason, the application of strip tillage should ideally be integrated with spatial traffic management strategies. The establishment of permanent traffic lanes or controlled traffic farming (CTF) systems can help confine mechanical loads to predefined corridors while preserving the loosened root-zone strip between vine rows. Such integration would increase the persistence of improved soil physical conditions and reduce the rate of re-compaction under repeated field operations typical for vineyard management [12,41].

The long-term effectiveness of localized strip tillage in vineyard systems is strongly influenced by machinery traffic patterns. In perennial crops such as vineyards, sprayers, harvesters and maintenance equipment repeatedly pass through the same inter-row corridors, generating cumulative soil compaction over time [12]. Under such conditions, the structural benefits produced by a single loosening operation may be progressively reduced if subsequent field operations occur directly above the treated strip. For this reason, the application of strip tillage should ideally be integrated with spatial traffic management strategies. The establishment of permanent traffic lanes or controlled traffic farming (CTF) systems can help confine mechanical loads to predefined corridors while preserving the loosened root-zone strips between vine rows. Such approaches are widely recognized as effective methods for limiting repeated soil compaction in mechanized perennial cropping systems, including vineyards [41,43]. By restricting wheel traffic to fixed tracks, CTF systems reduce cumulative soil stress and help maintain the structural improvements generated by localized deep loosening.

Another limitation of the present study concerns the soil type investigated. The experimental trials were conducted on light serozem soil of medium loam texture, which is characteristic of many irrigated vineyard regions of Central Asia. However, soil mechanical behaviour and soil–tool interaction processes depend strongly on texture, structure, carbonate content and moisture regime. Consequently, the magnitude of penetration resistance reduction, soil loosening efficiency and infiltration response observed in the present study may differ in soils with contrasting properties, such as heavy clay soils, gravelly soils or highly calcareous vineyard substrates. Similar variability of soil physical responses to tillage has been reported for vineyard soils under different management systems and environmental conditions [21,22,43]. Therefore, the results presented here should be interpreted primarily for soils with comparable texture and structural conditions. Additional experiments conducted on contrasting soil types would

be necessary to evaluate the robustness and wider applicability of the proposed strip-tillage geometry.

Another aspect that should be considered when interpreting the results concerns the operational applicability of the proposed strip-tillage implement in vineyards with different structural and spatial configurations. Vineyard production systems vary substantially in row spacing, slope gradient, soil depth and mechanization intensity. In the present study, the tool geometry and operating parameters were optimized for conditions typical of semi-arid vineyards with medium row spacing and relatively uniform terrain. In vineyards with narrow inter-row spacing, steep slopes or highly heterogeneous soil profiles, the operational parameters of the implement, including working depth, shank spacing and tool inclination angles, may require adjustment. Similar variability in soil response to tillage and mechanical soil disturbance has been reported in vineyard ecosystems under different management systems and environmental conditions [21,22,43]. Therefore, the proposed geometry should be interpreted as an optimized configuration for the tested conditions rather than as a universally fixed design. Future research should evaluate the performance of the implement across vineyards with contrasting row spacing, slope gradients and soil mechanical properties in order to determine the robustness and adaptability of the strip-tillage concept in different viticultural environments.

5. Conclusions

The observed relationships between tool geometry and soil responses should be interpreted within the context of coupled geometry–energy interactions during tillage.

This study demonstrates that geometry-driven optimization of a vineyard-specific strip tillage chisel tool can effectively improve soil physical quality and hydrologically relevant properties within the compacted root zone under the tested semi-arid conditions. The proposed U-shaped working body configuration, combining two oppositely inclined shanks with a central chisel, provided controlled fracture propagation within the trafficked strip while minimizing disturbance of the inter-row surface.

Field validation confirmed that targeted loosening in the 20–40 cm layer significantly reduced soil penetration resistance and bulk density, indicating improved mechanical conditions for root development. Simultaneously, the observed increase in infiltration rate suggests enhanced hydraulic continuity and improved vertical water movement. These changes should be interpreted as evidence of improved soil physical quality and hydraulic behavior rather than direct proof of broader soil health restoration or agronomic soil hydraulic function.

The results support the central hypothesis that optimized strip tillage can simultaneously: (i) alleviate subsoil compaction within the vineyard wheel-affected strip; (ii) enhance infiltration capacity and hydraulic functioning within the treated layer; and (iii) maintain operational feasibility through controlled soil disturbance. Unlike full-width subsoiling, the localized approach reduces unnecessary structural disruption, thereby aligning mechanical intervention with conservation-oriented soil and water management.

From a sustainability perspective, the integration of tool geometry optimization with soil physical and hydrological assessment provides a framework for evaluating tillage systems beyond draft performance alone. The study confirms that engineering design of soil-working elements should be quantitatively linked to measurable improvements in soil function, including root-zone permeability and structural stability. Such integration is essential for climate-resilient agriculture, particularly in vineyards exposed to repeated machinery traffic under semi-arid conditions.

The findings also indicate that strip-localized loosening may serve as a complementary strategy to biological soil management practices, such as cover cropping and

mulching, by addressing deeper mechanical constraints that surface-based methods cannot fully mitigate. Consequently, the proposed approach contributes to the development of sustainable and resource-efficient vineyard management systems.

Future research should focus on long-term monitoring of structural persistence and re-compaction dynamics, evaluation of grapevine physiological response and yield parameters, and assessment of energy consumption in relation to observed hydrological gains. Further work is also needed to adapt the optimized geometry to different soil textures and slope conditions. The integration of depth monitoring and precision control systems may further enhance reproducibility and field applicability.

In conclusion, the optimized strip tillage tool represents a viable engineering solution for improving soil physical quality and hydraulic function in vineyard agroecosystems under semi-arid conditions. The results indicate that the observed improvements in soil structure and water-related properties are associated with the combined interaction of tool geometry and energy transfer during tillage, rather than with geometry as an isolated factor. By linking implement design with measurable soil physical and hydrological responses, this study contributes to the conceptual and practical integration of agricultural machinery design with sustainable soil and water management. The long-term persistence of these improvements will depend on subsequent traffic management and the avoidance of repeated wheel loading over the mechanically loosened strip.

Author Contributions: Conceptualization, Y.S. and F.M. (Farmon Mamatov); methodology, Y.S., F.M. (Farmon Mamatov) and I.G.; software, Y.S. and A.S. (Antonina Sholoiko); validation, Y.S., F.M. (Farmon Mamatov) and A.S. (Antonina Sholoiko); formal analysis, Y.S. and A.S. (Antonina Sholoiko); investigation, I.G., D.I., K.R. and N.R.; resources, F.M. (Farmon Mamatov), D.I., K.R., G.E., Y.R., F.M. (Feruza Mukumova), A.S. (Alisher Suyunov) and B.A.; data curation, I.G., D.I. and N.R.; writing—original draft preparation, Y.S.; writing—review and editing, Y.S., F.M. (Farmon Mamatov), A.S. (Antonina Sholoiko) and I.G.; visualization, Y.S. and A.S. (Antonina Sholoiko); supervision, Y.S. and F.M. (Farmon Mamatov); project administration, Y.S.; funding acquisition, F.M. (Farmon Mamatov) and Y.S. All authors have read and agreed to the published version of the manuscript.

Funding: This research was carried out within the framework of the project No. 5.2.1.1.i.0/2/24/I/CFLA/002 (AF-12) "Strengthening the institutional capacity of Latvia University of Life Sciences and Technologies to ensure excellence in education and research" (Contract No. 3.2.-10/197).

Data Availability Statement: The data presented in this study are available from the corresponding author upon reasonable request. The datasets are not publicly available due to ongoing extended research activities and institutional research agreements related to continuing field experiments. The data form part of a broader longitudinal study on vineyard soil structural and hydrological dynamics.

Acknowledgments: The authors sincerely thank the staff of the Agrihorts Institute for providing experimental facilities and technical support. No generative AI or AI-assisted technologies were used during the preparation of this work.

Conflicts of Interest: The authors declare no conflicts of interest.

Nomenclature

a	working depth of the chisel tool (m)
α, α_i	chisel entry (crushing) angle to the horizontal (°)
β_b	inclination angle of the shank in the longitudinal vertical plane (°)

β_k	inclination angle of the shank in the transverse vertical plane (°)
b_i	width of the chisel (m)
B_q	spacing between side shanks (m)
$F_{<50}$	soil-crushing efficiency (percentage of aggregates < 50 mm, %)
g	gravitational acceleration (9.81 m·s^{-2})
H	total height of the shank (m)
h_1	clearance between the frame and the loosened soil surface (m)
h_2	ridge height of loosened soil above ground level (m)
h_b, h_{ib}	local soil height parameters in the crushing zone (m)
I	empirical coefficient of loosening (–)
L, L_i	length of the chisel (m)
q_0	empirical soil strength coefficient (–)
ρ	bulk soil density (kg·m^{-3})
T_e	specific soil compression resistance (Pa)
τ	shear strength of soil (Pa)
φ	soil–metal friction angle (°)
φ_1	internal soil friction angle (°)
ψ_k	auxiliary angle of shank inclination in transverse plane (°)
γ	angle between inclined shanks (°)
ε	soil crushing coefficient (–)
V	forward speed of tool (km·h^{-1})
X_1–X_5	coded factors in regression models (–)
Y_1	soil-crushing efficiency (%, response function)
Y_2	draft resistance (kN, response function)

References

1. Aldoshin, N.V.; Mamatov, F.M.; Kuznetsov, Y.A.; Kravchenko, I.N.; Kupreenko, A.I.; Ismailov, I.J.; Kalashnikova, L.V. Loosening and leveling device for preparing soil for melon crops. *INMATEH-Agric. Eng.* **2021**, *64*, 269–278. https://doi.org/10.35633/inmateh-64-26.
2. Aldoshin, N.; Mamatov, F.; Ismailov, I.; Ergashov, G. Development of combined tillage tool for melon cultivation. In *19th International Scientific Conference Engineering for Rural Development*; Latvia University of Life Sciences and Technologies: Jelgava, Latvia, 2020; pp. 767–772. https://doi.org/10.22616/ERDev.2020.19.TF175.
3. Mirzaev, B.; Mamatov, F.; Tursunov, O. A justification of broach-plow's parameters of the ridge-stepped ploughing. *E3S Web Conf.* **2019**, *97*, 05035. https://doi.org/10.1051/e3sconf/20199705035.
4. Mamatov, F.M.; Rajabov, Y.; Temirov, I.G.; Chuyanov, D.S. Parameters of the ripper-mole knife. *AIP Conf. Proc.* **2024**, *2969*, 060025. https://doi.org/10.1063/5.0183490.
5. Shevchenko, I.; Golub, G.; Tsyvenkova, N.; Shevchenko, I.; Titova, L.; Omarov, I.; Zayets, M. Substantiating the structural and technological parameters of tillage rotary x-like working bodies. *East. Eur. J. Enterp. Technol.* **2024**, *130*, 45–53. https://doi.org/10.15587/1729-4061.2024.309756.
6. Patuk, I.; Borowski, P. Computer aided engineering design in the development of agricultural implements: A case study for a DPFA. *J. Phys. Conf. Ser.* **2020**, *1679*, 052005. https://doi.org/10.1088/1742-6596/1679/5/052005.
7. Patuk, I.; Hasegawa, H.; Borodin, I.; Whitaker, A.C.; Borowski, P.F. Simulation for design and material selection of a deep placement fertilizer applicator for soybean cultivation. *Open Eng.* **2020**, *10*, 733–743. https://doi.org/10.1515/eng-2020-0082.
8. Syromyatnikov, Y.N.; Orekhovskaya, A.A.; Dzjasheev, A.; Kalimullin, M.N.; Tikhonov, E.A.; Luchinovich, A.A.; Bielykh, A.V. Cultivator points of the rotary tillage loosening and separating machine of the stratifier. *J. Phys. Conf. Ser.* **2021**, *2094*, 042024. https://doi.org/10.1088/1742-6596/2094/4/042024.
9. Nukeshev, S.; Yeskhozhin, K.; Karaivanov, D.; Ramaniuk, M.; Akhmetov, E.; Saktaganov, B.; Tanbayev, K. A chisel fertilizer for in-soil tree-layer site-specific application in precision farming. *Int. J. Technol.* **2021**, *14*, 109–118. https://doi.org/10.14716/ijtech.v14i1.5143.
10. Shablia, V.P.; Tkachova, I.V. Machine and manual working actions for different manure removing technologies. *Bol. Ind. Anim.* **2020**, *77*, e1482. https://doi.org/10.17523/bia.2020.v77.e1482.
11. de Medeiros, S.F.; Tavares, R.L.M.; Ferreira, C.J.B.; Rosa, M.; de Souza, G.S.; Boldrin, P.F.; da Silva Júnior, J.F. Straw use to reducing soil compaction and its effect on the biometric and physiological characteristics of soybean and maize plants. *Commun. Soil Sci. Plant Anal.* **2024**, *55*, 1956–1966. https://doi.org/10.1080/00103624.2024.2336569.

12. Mojžiš, M.; Jobbágy, J.; Rataj, V.; Zsembeli, J. Impact of machinery passages on soil compaction in field conditions. *Acta Technol. Agric.* **2024**, *27*, 116–124. https://doi.org/10.2478/ata-2024-0016.
13. Mwiti, F.M.; Gitau, A.N.; Mbuge, D.O. Edaphic response and behavior of agricultural soils to mechanical perturbation in tillage. *AgriEngineering* **2022**, *4*, 335–355. https://doi.org/10.3390/agriengineering4020023.
14. Syromyatnikov, Y.; Troyanovskaya, I.; Zagidullin, R.; Tikhonov, E.; Orekhovskaya, A.; Voinash, S. Soil density in traditional mouldboard tillage. *Acta Technol. Agric.* **2023**, *26*, 159–165. https://doi.org/10.2478/ata-2023-0021.
15. Liu, T.Q.; Fan, D.J.; Zhang, X.X.; Chen, J.; Li, C.F.; Cao, C.G. Deep placement of nitrogen fertilizers reduces ammonia volatilization and increases nitrogen utilization efficiency in no-tillage paddy fields in central China. *Field Crops Res.* **2015**, *184*, 80–90. https://doi.org/10.1016/j.fcr.2015.09.011.
16. Mazid Miah, M.A.; Gaihre, Y.K.; Hunter, G.; Singh, U.; Hossain, S.A. Fertilizer deep placement increases rice production: Evidence from farmers' fields in southern Bangladesh. *Agron. J.* **2016**, *108*, 805–812. https://doi.org/10.2134/agronj2015.0170.
17. Korotkova, I.; Marenych, M.; Hanhur, V.; Laslo, O.; Chetveryk, O.; Liashenko, V. Weed control and winter wheat crop yield with the application of herbicides, nitrogen fertilizers, and their mixtures with humic growth regulators. *Acta Agrobot.* **2021**, *74*, 1. https://doi.org/10.5586/aa.748.
18. Chuyanov, D.S.; Mamatov, F.M.; Shodmonov, G.D. Main parameters of manure sealer. *E3S Web Conf.* **2023**, *401*, 04031. https://doi.org/10.1051/e3sconf/202340104031.
19. Kuts, O.; Kokoiko, V.; Mykhailyn, V.; Syromyatnikov, Y.; Zhernova, O. Fertilisation system influence on the main agrochemical indicators of soil and productivity of white cabbage. *Sci. Horiz.* **2023**, *26*, 69–79. https://doi.org/10.48077/scihor11.2023.69.
20. Kuts, O.; Kokoiko, V.; Semenenko, S.; Semenenko, I.; Romanov, V. The impact of biologically enhanced fertilisation systems on sweet potato productivity and quality. *Sci. Horiz.* **2024**, *27*, 64–72. https://doi.org/10.48077/scihor9.2024.64.
21. Novara, A.; Stallone, G.; Cerdà, A.; Gristina, L. The effect of shallow tillage on soil erosion in a semi-arid vineyard. *Agronomy* **2019**, *9*, 257. https://doi.org/10.3390/agronomy9050257.
22. Buesa, I.; Mirás-Avalos, J.; Paz, J.; Visconti, F.; Sanz, F.; Yeves, A.; Guerra, D.; Intrigliolo, D. Soil management in semi-arid vineyards: Combined effects of organic mulching and no-tillage under different water regimes. *Eur. J. Agron.* **2021**, *123*, 126198. https://doi.org/10.1016/j.eja.2020.126198.
23. Li, C.; Li, M.; Xiong, T.; Yang, H.; Peng, X.; Wang, Y.; Qin, H.; Li, H.; Tang, Y.; Fan, G. Strip tillage improves productivity of direct-seeded oilseed rape in rice–oilseed rape rotation systems. *Agriculture* **2024**, *14*, 1356. https://doi.org/10.3390/agriculture14081356.
24. Hu, K.; Zhang, W.; Qi, B.; Ji, Y. Tillage depth dynamic monitoring and precise control system. *Meas. Control* **2025**, *58*, 394–403. https://doi.org/10.1177/00202940241263454.
25. Lü, J.; Cui, P.; Zhu, X.; Qi, Y.; Yang, D.; Sun, Q. Optimal design and test of longitudinal and lateral stability of large monopoly wide potato cultivator. *Trans. Chin. Soc. Agric. Mach.* **2023**, *54*, 88–96.
26. Ushakov, A.E. Estimation of the operating efficiency of deep loosening soil tillage elements using the rational utilisation factor. *Agric. Eng.* **2023**, *5*, 40–45. https://doi.org/10.26897/2687-1149-2023-5-40-45.
27. Xu, X.; Jing, P.; Yao, Q.; Chen, W.; Meng, H.; Li, X.; Qi, J.; Peng, H. Parameter optimization and test for the pulse-type gas explosion subsoiler. *Agriculture* **2024**, *14*, 1417. https://doi.org/10.3390/agriculture14081417.
28. Chen, X.; Xu, G.; Zhang, X.; Tan, W.; Ding, Q.; Tagar, A.A. Performance evaluation of biomimetic-designed rotary blades for straw incorporation in an intensive tillage system. *Agriculture* **2024**, *14*, 1426. https://doi.org/10.3390/agriculture14081426.
29. Buivydienė, A.; Deveikytė, I.; Veršulienė, A.; Feiza, V. Tillage practices effect on root distribution and variation of soil CO_2 emission under different cropping strategies. *Agronomy* **2024**, *14*, 1768. https://doi.org/10.3390/agronomy14081768.
30. Shen, H.; Hu, W.; Che, X.; Li, C.; Liang, Y.; Wei, X. Assessment of effectiveness and suitability of soil and water conservation measures on hillslopes of the Black Soil Region in Northeast China. *Agronomy* **2024**, *14*, 1755. https://doi.org/10.3390/agronomy14081755.
31. Modiba, M.M.; Ocansey, C.M.; Ibrahim, H.T.M.; Birkás, M.; Dekemati, I.; Simon, B. Assessing the impact of tillage methods on soil moisture content and crop yield in Hungary. *Agronomy* **2024**, *14*, 1606. https://doi.org/10.3390/agronomy14081606.
32. Syromyatnikov, Y.; Orekhovskaya, A.; Klyosov, D.; Vodolazskaya, N.; Syromyatnikov, P.; Sementsov, V. Field tests of the experimental installation for soil processing. *J. Terramech.* **2022**, *100*, 81–86. https://doi.org/10.1016/j.jterra.2022.01.004.
33. Syromyatnikov, Y.N.; Orekhovskaya, A.A.; Dzjasheev, A.; Tikhonov, E.A.; Kalimullin, M.N.; Ivanov, A.A.; Sokolova, V.A. Improving stability of movement of machine section for soil preparation and seeding. *J. Phys. Conf. Ser.* **2021**, *2094*, 042027. https://doi.org/10.1088/1742-6596/2094/4/042027.

34. Pashchenko, V.F.; Syromyatnikov, Y.N. The transporting ability of the rotor of the soil-cultivating loosening and separating vehicle. *Tractors Agric. Mach.* **2019**, *86*, 67–74. https://doi.org/10.31992/0321-4443-2019-2-67-74.
35. Shukhanov, S.N.; Dorzhiev, A.S.; Kosareva, A.V. The results of experimental studies of the root crop chopper. *Tractors Agric. Mach.* **2020**, *87*, 56–61. https://doi.org/10.31992/0321-4443-2020-1-56-61.
36. Wang, Y.; Song, Z.; Abdullahi, H.S.; Gao, S.; Zhang, H.; Zhou, L.; Li, Y. A lightweight detection algorithm for surface defects in small-sized bearings. *Electronics* **2024**, *13*, 2614. https://doi.org/10.3390/electronics13132614.
37. *ISO 7256-1:1984*; *Agricultural Machinery—Test Procedures for Tillage and Soil-Working Equipment—Part 1: General*. ISO: Geneva, Switzerland, 1984.
38. Cataldo, D.; Paoletti, A.; Novara, A.; Saia, S. Soil management, sustainable strategies and approaches to improve the quality of modern viticulture. *Agronomy* **2021**, *11*, 2359. https://doi.org/10.3390/agronomy11112359.
39. Silvestroni, O.; Di Nasso, N.N.; Moreschini, L.; Bonari, E. Using legume-enriched cover crops to improve grape yield and quality in hillside vineyards. *Agronomy* **2024**, *14*, 2528. https://doi.org/10.3390/agronomy14112528.
40. Pornaro, C.; Poesen, J.; Salvador, S.; Strauss, P. Selection of inter-row herbaceous covers in a sloping, organic, non-irrigated vineyard. *PLoS ONE* **2022**, *17*, e0279759. https://doi.org/10.1371/journal.pone.0279759.
41. Pessina, D.; Facchinetti, D.; Greppi, P. Sustainability of machinery traffic in vineyard. *Sustainability* **2021**, *13*, 2475. https://doi.org/10.3390/su13052475.
42. Diti, I.; Novara, A.; Saia, S.; Gristina, L. A new integrated approach for management of soil threats in the vineyard ecosystem. *Catena* **2020**, *194*, 104788. https://doi.org/10.1016/j.catena.2020.104788.
43. Telak, L.J.; Bogunović, I. Tillage-induced impacts on the soil properties, soil water erosion, and loss of nutrients in the vineyard. *J. Cent. Eur. Agric.* **2020**, *21*, 660–674. https://doi.org/10.5513/jcea01/21.3.2810.
44. Novara, A.; Gristina, L.; Saia, S.; Cerdà, A. Soil carbon budget account for the sustainability improvement of a Mediterranean vineyard area. *Agronomy* **2020**, *10*, 336. https://doi.org/10.3390/agronomy10030336.
45. Parkhomenko, A.V.; Kambulov, A.M. Multi-purpose chisel for soil treatment in vineyards. *Russian Vine* **2021**, *17*, 31–39. https://doi.org/10.32904/2712-8245-2021-17-31-39.
46. Cabrera-Pérez, M.Á.; García-Díaz, A.; Martín-Lammerding, D. Organic mulches as an alternative to conventional under-vine weed management in Mediterranean vineyards. *Plants* **2022**, *11*, 2785. https://doi.org/10.3390/plants11202785.
47. Kaya, A.; Sezgin, F.H.; Öz, H. Improving organic grape production: The effects of soil management and organic fertilizers. *Chem. Biol. Technol. Agric.* **2024**, *11*, 33. https://doi.org/10.1186/s40538-024-00564-2.

Disclaimer/Publisher's Note: The statements, opinions and data contained in all publications are solely those of the individual author(s) and contributor(s) and not of MDPI and/or the editor(s). MDPI and/or the editor(s) disclaim responsibility for any injury to people or property resulting from any ideas, methods, instructions or products referred to in the content.